Precambrian Research 165 (2008) 221–242

Contents lists available at ScienceDirect

Precambrian Research

journal homepage: www.elsevier.com/locate/precamres

# Geochemistry and zircon geochronology of paleoproterozoic granitoids: Further evidence on the magmatic and crustal evolution of the São Luís cratonic fragment, Brazil

Evandro L. Klein[a,*], Renê Luzardo[b], Candido A.V. Moura[c], Richard Armstrong[d]

[a] CPRM/Geological Survey of Brazil – Av. Dr. Freitas 3645, Belém-PA CEP 66095-110, Brazil
[b] CPRM/Geological Survey of Brazil – Av. André Araújo 2160, Manaus-AM CEP 69060-001, Brazil
[c] Universidade Federal do Pará, Centro de Geociências, CP 1611, Belém-PA CEP 66075-900, Brazil
[d] Research School of Earth Sciences, Mills Road, The Australian National University, Canberra 0200, Australia

ARTICLE INFO

*Article history:*
Received 22 February 2008
Received in revised form 11 May 2008
Accepted 17 July 2008

*Keywords:*
São Luís cratonic fragment
Geochemistry
Paleoproterozoic
Geochronology
Granitoid
Calc-alkaline

ABSTRACT

The Tromaí Intrusive Suite is the predominant exposed unit of the São Luís cratonic fragment in northern Brazil. The suite forms batholiths and stocks of granitoids that were emplaced between 2168 ± 4 Ma and 2149 ± 4 Ma and intruded a 2240 ± 5 Ma old metavolcano-sedimentary sequence. The batholiths are composed of a variety of petrographic types that have been grouped in three sub-units, based on the predominant petrographic type, and named Cavala Tonalite, Bom Jesus Granodiorite, and Areal Granite, from the more primitive to the more evolved phases, in addition to subordinate shallow felsic intrusions. The Tromaí Suite is an expanded magmatic association comprising minor mafic rocks to predominantly intermediate and felsic, low- to high-K, and metaluminous to weakly peraluminous granitoids that follow a Na-enriched calc-alkaline trend. Combined rock association, geochronology, Nd isotopes, and geochemical signature indicate that the Tromaí Suite formed from magmas derived from juvenile protoliths modified by fractional crystallization. The juvenile protoliths included ocean plate, mantle wedge, and minor sediments. The data also indicate an intra-oceanic arc setting that possibly transitioned to a continental margin and that the Tromaí Intrusive Suite records the main accretionary stage of the Rhyacian orogen (ca. 2.24–2.15 Ma) that culminated with a collision stage at about 2.1 Ga and gave rise to the present day São Luís cratonic fragment. This time interval is coincident with the main period of crustal growth in the South American Platform and in the Paleoproterozoic terranes of the West African Craton. The beginning of this period is also coincident with the end of a period in which only minor amounts of juvenile crust is found worldwide.

The Negra Velha Granite is a distinct unit that forms a few stocks that intruded the granitoids of the Tromaí Suite between 2076 and 2056 Ma ago. Negra Velha is an association of monzogranite and subordinate quartz–monzonite and syenogranite with an alkaline signature that shows high Rb–Sr–Ba enrichments, resembling shoshonitic associations. This granite represents the post-orogenic phase of the Rhyacian orogenesis.



## 1. Introduction

Based on Nd data from granitoids, Cordani and Sato (1999) concluded that the main period of crust formation in the South American Platform was between 2.2 Ga and 2.0 Ga, which corresponds to the time interval of the Trans-Amazonian cycle of orogenies. Most of these juvenile terranes are concentrated in northern Brazil, especially in the Amazonian Craton, but also include the São Luís cratonic fragment and parts of the basement of Neoproterozoic belts. The beginning of this interval overlaps with the end of a period during which Condie (2000) and Condie et al. (2005) verified a worldwide paucity of juvenile crust.

Paleoproterozoic granitoids represent over 80% of the exposed lithological framework of the São Luís cratonic fragment in northern Brazil (Fig. 1). Two distinct phases of emplacement have been described so far. The majority of the granitoids belong to the Tromaí Intrusive Suite that have ages between 2147 ± 3 Ma and 2168 ± 4 Ma and Sm–Nd $T_{DM}$ ages of 2.23–2.26 Ga (Klein and Moura, 2001, 2003;

* Corresponding author at: CPRM/Geological Survey of Brazil – Av. Dr. Freitas 3645, Belém-PA CEP 66095-110, Brazil. Tel.: +55 91 3182 1334; fax: +55 91 3276 4020.
*E-mail address:* eklein@be.cprm.gov.br (E.L. Klein).

0301-9268/$ – see front matter © 2008 Elsevier B.V. All rights reserved.
doi:10.1016/j.precamres.2008.07.005

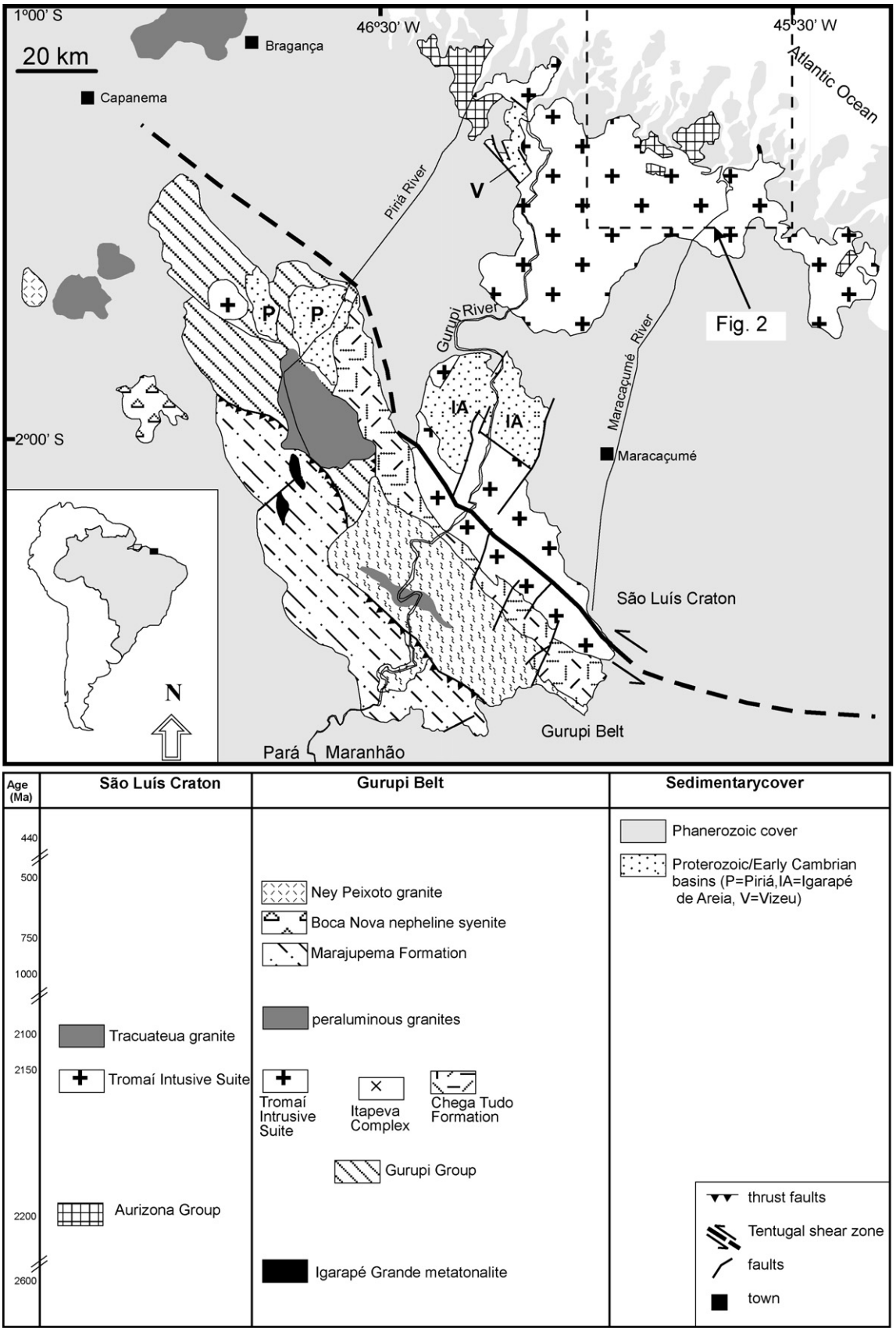


**Fig. 1.** Geologic map of the São Luís Craton and Gurupi Belt and location of the study area (arrow).

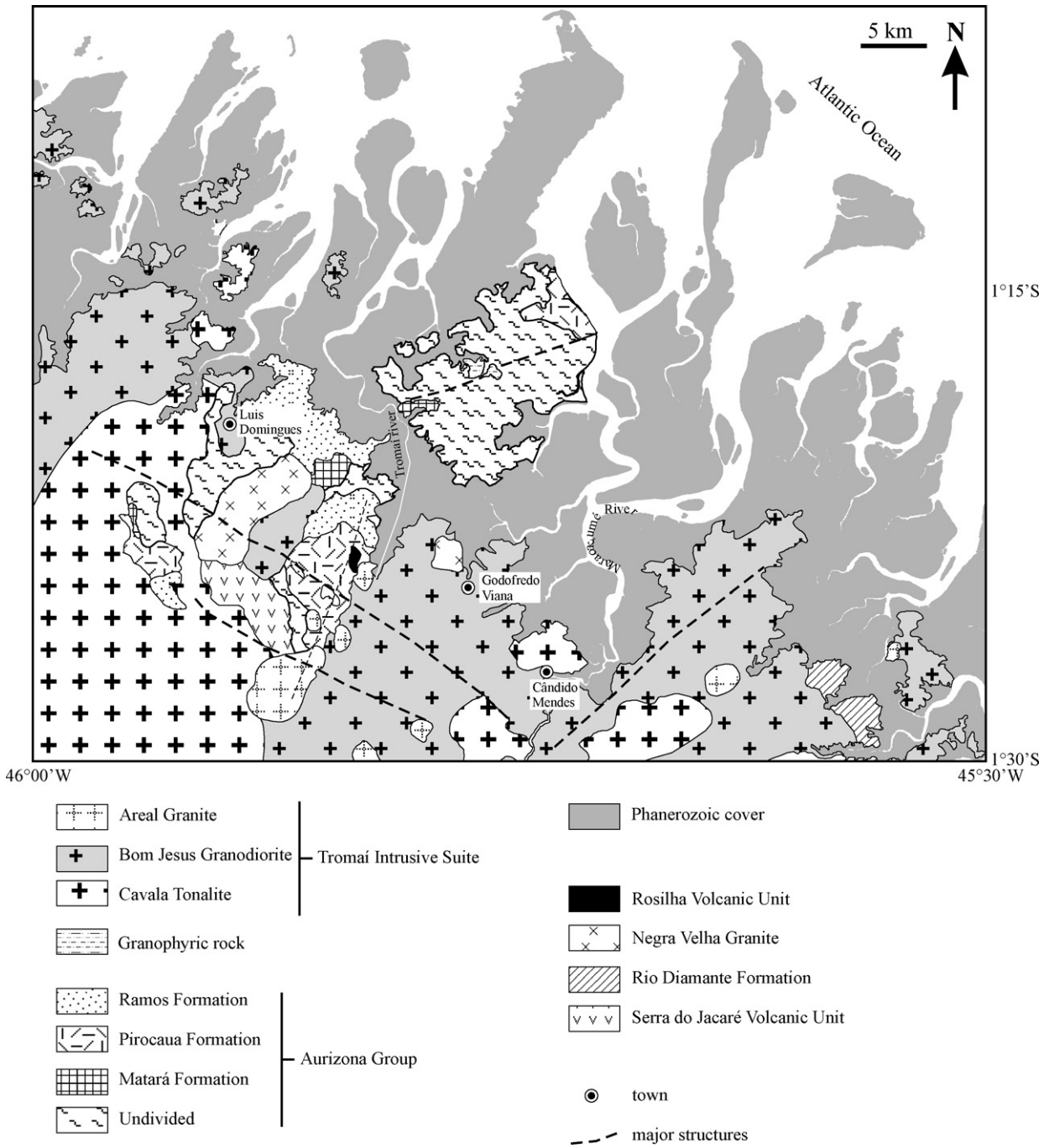


**Fig. 2.** Geologic map of the study area in the central portion of the São Luís Craton (adapted from Klein et al., 2008b).

Klein et al., 2005a). These granitoids occur in close association with coeval volcanic rocks and a 2240 ± 5 Ma old metavolcano-sedimentary sequence (Figs. 1 and 2). A subordinate association is composed of peraluminous, S-type granitoids (Lowell, 1985) of the Tracuateua Intrusive Suite, with ages between 2086 ± 10 Ma and 2091 ± 5 Ma (Palheta, 2001).

The geochemistry and petrogenesis of the Tracuateua Suite is well described (Lowell, 1985). On the other hand, the understanding of the Tromaí Intrusive Suite is still limited. Originally, this suite was defined as an anorogenic plutonic–volcanic association (Costa et al., 1977). Later, Pastana (1995) kept the concept of plutonic–volcanic association and described the granitoids of the Tromaí Intrusive Suite as low-K, calc-alkaline, I-type, peraluminous rocks produced by the partial melting of a supposed amphibolitic lower crust, and resembling Archean TTG suites. Pastana (1995) also stated that the emplacement of the granitoids was post-tectonic occurring in an extensional regime within a convergent plate margin, probably because of the absence of important tectonic deformation imprinted in rocks of this suite. Klein et al. (2005a), based on zircon geochronology, Nd isotopes, and in the review of the limited geochemical data presented by Pastana (1995), reinterpreted the Tromaí Suite to be composed of juvenile orogenic rocks, observing characteristics of both calc-alkaline and TTG associations, and interpreted the granitoids to have formed in intra-oceanic island arcs with protoliths derived from the mantle wedge and/or subducted oceanic crust.

In this paper we refine the characterization of the Tromaí Intrusive Suite and describe another granitic association recently recognized in the São Luís cratonic fragment. This is based on recent field work undertaken in the central portion of the cratonic area (Figs. 1 and 2), petrography, new whole rock geochemical data and additional zircon geochronology. The results allow us to address the magmatic evolution and tectonic setting of the granitoid rocks of the São Luís cratonic fragment and the implications for the crustal evolution of this geotectonic unit. Additional points that are addressed are the significance of the results to the evolution of the South American Platform and to global correlations.

## 2. Geologic overview

The São Luís cratonic fragment is composed predominantly of granitoids of variable composition and ages and subordinate supracrustal rocks. The oldest rocks belong to the metavolcanic-sedimentary sequence of the Aurizona Group dated at 2240 ± 5 Ma (Klein and Moura, 2001). This sequence comprises a calc-alkaline felsic unit with metavolcanic and metapyroclastic rocks, a tholeiitic to high-K calc-alkaline metamafic–metaultramafic unit, and a metasedimentary sequence (Klein et al., 2008a). The metamorphism attained dominantly the greenschist facies, and locally amphibolite facies (Pastana, 1995; Klein et al., 2008b). Klein et al. (2008a) interpreted this supracrustal sequence to have formed in a volcanic arc and to have minor back-arc components. The Aurizona Group was intruded by granophyric rocks at 2214 ± 3 Ma (Klein et al., 2008b).

Most of the granitoids of the cratonic area are attributed to the Tromaí Intrusive Suite (Fig. 1). The suite is composed of granitoids of variable composition that form batholiths, stocks, and subordinate shallow intrusions and dikes. This suite is subdivided here into three units, termed Cavala Tonalite, Bom Jesus Granodiorite, and Areal Granite (Fig. 2), based on mineralogical and structural characteristics and in the predominance of the rock type (see next section). Previous geochronology showed that, as a whole, the suite has ages between 2168 Ma and 2147 Ma and juvenile Nd signature (Klein and Moura, 2001, 2003; Klein et al., 2005a). Another granitoid unit has been identified by Klein et al. (2008a) and named Negra Velha Granite, which has been considered to be younger than the Tromaí Suite.

The Tracuateua Intrusive Suite crops out in the westernmost known portion of the São Luís cratonic fragment (Fig. 1). The suite is composed of foliated biotite- and muscovite-bearing syenogranites and monzogranites that host enclaves of schist, gneiss, and migmatite and show a peraluminous, S-type signature (Lowell, 1985). These rocks have been emplaced between 2086 ± 10 Ma and 2091 ± 5 Ma (Palheta, 2001).

Three units of volcanic rocks occur in close spatial association with the Tromaí granitoids and the Aurizona Group (Fig. 2). These are mostly felsic to intermediate rocks, sometimes showing tuffaceous components, and subordinate mafic phases, which formed at 2164 Ma, 2160 Ma, and 2068 Ma (Klein et al., 2008a). The oldest unit (Serra do Jacaré Volcanic Unit) comprises mainly metaluminous, calc-alkaline andesite to minor tholeiitic basalt and is interpreted to have formed in mature arc or continental margin, with limited back-arc components. The 2160 Ma old unit (Rio Diamante Formation) is composed of metaluminous, medium-K calc-alkaline dacite porphyry and tuff that record continental margin or transitional environment. The youngest volcanic unit recognized so far

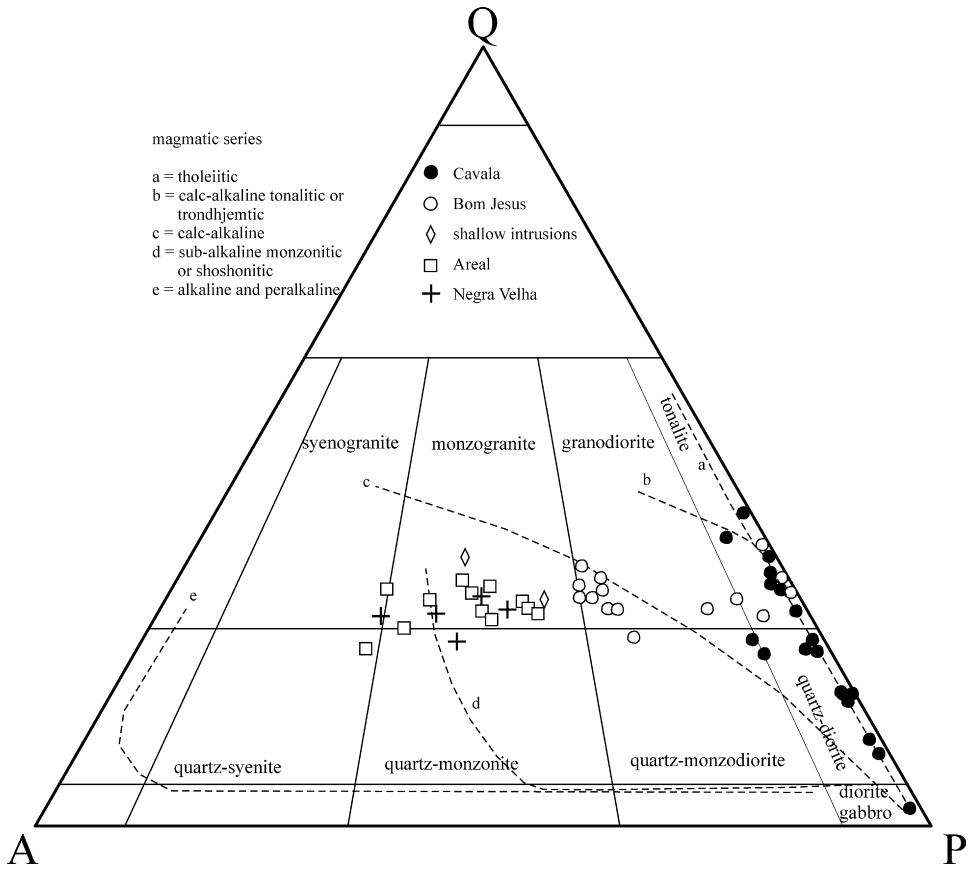


**Fig. 3.** QAP diagram (Streckeisen, 1976) with chemical trends (dashed arrows) of Lameyre and Bowden (1982) for the granitoids of the Tromaí Intrusive Suite and Negra Velha Granite.

**Table 1a**
Modal compositions of samples from the Cavala Tonalite

| | TF7E dio/gab | EK148 dio | EK1 qzdio | EK98 qzdio/ton | EK100 qzdio | TF24A ton | EK32A qzmzdio | EK150A qzdio | EK06A ton |
|---|---|---|---|---|---|---|---|---|---|
| Quartz | 5 | <1 | 13 | 20 | 20 | 27 | 15 | 15 | 25 |
| Plagioclase | 40 | 46 | 45 | 45 | 45 | 40 | 48 | 49 | 54 |
| Microcline | nd | nd | nd | <1 | <1 | <1 | 5 | - | <1 |
| Hornblende | 18 | 49 | 35 | 30 | 29 | 10 | 29 | 35 | 20 |
| Pyroxene | 30 | <0.1 | nd | nd | nd | nd | nd | nd | nd |
| Biotite | <1 | nd | 1 | nd | nd | 1 | nd | nd | nd |
| Chlorite | <1 | <1 | <1 | <1 | <1 | 18 | <1 | <1 | <1 |
| Opaque | 6 | 3 | 4 | 3 | 4 | 3 | 2 | <1 | <1 |
| Sericite | <1 | <1 | <1 | <1 | <1 | <1 | <1 | <1 | <1 |
| Titanite | <1 | nd | <1 | <1 | <1 | <1 | <1 | <1 | <1 |
| Apatite | <1 | 1 | 1 | 1 | 1 | <1 | <1 | <1 | <1 |
| Zircon | nd | nd | nd | <1 | <1 | nd | nd | <1 | <1 |
| Epidote | <1 | <1 | <1 | <1 | nd | <1 | <1 | <1 | <1 |
| Tourmaline | nd | nd | nd | nd | nd | nd | nd | nd | nd |
| Calcite | nd | <0.1 | <1 | <1 | <0.1 | nd | <1 | nd | nd |
| Allanite | nd | nd | nd | nd | nd | nd | nd | nd | nd |
| Prehnite | nd | nd | nd | nd | nd | nd | nd | nd | nd |
| Fluorite | nd | nd | nd | nd | nd | nd | nd | nd | nd |
| Rutile | nd | nd | nd | nd | nd | nd | nd | nd | nd |

**Table 1b**
Modal compositions of samples from the Bom Jesus Granodiorite and associated shallow intrusions

| | EK167A ton | EK25 ton | TF12 ton | EK164A gdr | EK189 ton | EK188 ton | EK142A gdr | EK147A gdr | EK19A mzgra | EK163 mzgra | EK30 aplite |
|---|---|---|---|---|---|---|---|---|---|---|---|
| Quartz | 25 | 30 | 30 | 29 | 30 | 20 | 25 | 22 | 26 | 25 | 30 |
| Plagioclase | 40 | 59 | 52 | 40 | 59 | 45 | 40 | 52 | 39 | 33 | 27 |
| Microcline | 20 | nd | nd | 20 | nd | nd | 20 | 20 | 30 | 33 | 30 |
| Hornblende | 14 | nd | nd | nd | nd | 34 | nd | nd | nd | 8 | 10 |
| Pyroxene | nd | nd | nd | nd | nd | nd | nd | nd | nd | nd | nd |
| Biotite | nd | 10 | 15 | 10 | 6 | <1 | 14 | 5 | 4 | <1 | nd |
| Chlorite | <1 | <1 | <1 | <1 | <1 | <1 | <1 | <1 | <1 | <1 | <1 |
| Opaque | <1 | <1 | nd | <1 | 2 | <1 | <1 | <1 | <1 | <1 | 2 |
| Sericite | <1 | <1 | <1 | <1 | <1 | <1 | <1 | <1 | <1 | <1 | <1 |
| Titanite | <1 | <1 | 2 | <1 | 2 | <1 | <1 | <1 | <1 | <1 | <1 |
| Apatite | <1 | <1 | <1 | <1 | <1 | <1 | <1 | <1 | <1 | <1 | <1 |
| Zircon | <1 | nd | nd | <1 | <1 | <1 | nd | <1 | nd | nd | nd |
| Epidote | <1 | <1 | <1 | <1 | <1 | nd | <1 | <1 | <1 | <1 | <1 |
| Tourmaline | nd | nd | nd | nd | nd | nd | nd | nd | nd | nd | nd |
| Calcite | <1 | <1 | nd | <1 | <1 | nd | nd | nd | <1 | <1 | <1 |
| Allanite | nd | nd | nd | <1 | nd | nd | nd | nd | <1 | nd | nd |
| Prehnite | nd | nd | nd | nd | <0.1 | nd | nd | nd | nd | nd | nd |
| Fluorite | nd | nd | nd | nd | nd | nd | nd | nd | nd | nd | nd |
| Rutile | nd | nd | nd | nd | nd | nd | nd | nd | <1 | nd | nd |

**Table 1c**
Modal compositions of samples from the Areal Granite and Negra Velha Granite

| | Areal Granite | | | | Negra Velha Granite | | |
|---|---|---|---|---|---|---|---|
| | EK190 mzgra | EK178 mzgra | EK162 sygra | EK33 sygra | EK20 qzmzo | EK15 mzgra | EK81 sygra |
| Quartz | 28 | 27 | 22 | 29 | 20 | 25 | 24 |
| Plagioclase | 33 | 39 | 25 | 24 | 30 | 30 | 25 |
| Microcline | 35 | 30 | 49 | 43 | 35 | 30 | 45 |
| Hornblende | nd | nd | nd | nd | 10 | 9 | nd |
| Pyroxene | nd | nd | nd | nd | nd | nd | nd |
| Biotite | 3 | 3 | 3 | 3 | 3 | 5 | 5 |
| Chlorite | <1 | <1 | <1 | <1 | <1 | <1 | <1 |
| Opaque | <1 | <1 | <1 | <1 | nd | <1 | <1 |
| Sericite | <1 | <1 | <1 | <1 | <1 | <1 | <1 |
| Titanite | nd | nd | <1 | nd | 1 | <1 | <1 |
| Apatite | <1 | <1 | nd | <1 | <1 | <1 | <1 |
| Zircon | nd | <1 | <1 | <1 | nd | <1 | <1 |
| Epidote | nd | <1 | <1 | <1 | <1 | <1 | <1 |
| Tourmaline | nd | nd | nd | nd | <1 | nd | <1 |
| Calcite | <1 | nd | nd | nd | nd | <1 | nd |
| Allanite | <1 | <1 | <1 | nd | nd | nd | <1 |
| Prehnite | nd | nd | nd | nd | nd | nd | nd |
| Fluorite | nd | nd | nd | nd | nd | <1 | nd |
| Rutile | nd | nd | nd | nd | nd | nd | nd |

nd: not determined. Rock names abbreviations: dio, diorite; gab, gabbro; gdr, granodiorite; mzgra, monzogranite; qzdio, quartz-diorite; qzmzdio, quartz-monzodiorite; qzmzo, quartz-monzonite; sygra, syenogranite.

**Table 2**
Summary of available geochronological and Nd isotopes data for the granitoids of the São Luís cratonic fragment

| Granitoid unit | Rock type | Age (Ma) | $T_{DM}$ (Ga) | εNd(t) | Reference |
|---|---|---|---|---|---|
| TIS[a]/Cavala tonalite | Tonalite | 2168 ± 4 | 2.26 | +2.2 | Klein et al. (2005a) |
| | Tonalite | 2165 ± 2 | | | Klein and Moura (2001) |
| | Tonalite | 2160 ± 2 | | | Klein et al. (2005a) |
| TIS/Bom Jesus granodiorite | Monzogranite | 2152 ± 3 | 2.23 | +2.3 | Klein and Moura (2001, 2003) |
| TIS/Areal granite | Monzogranite | 2163 ± 3 | 2.22 | +2.6 | Klein et al. (2005a), Klein and Moura (2001) |
| | Syenogranite | 2149 ± 4 | 2.26 | +1.9 | Klein et al. (2005a), Klein and Moura (2003) |
| Tracuateua Suite | Granite | 2091 ± 5 | 2.31–2.32 | +1.1 to +1.0 | Palheta (2001) |
| | Granite | 2086 ± 10 | 2.46–2.50 | +0.2 to −1.3 | Palheta (2001) |

[a] TIS: Tromaí Intrusive Suite.

(Rosilha Volcanic Unit), comprises weakly peraluminous, high-K calc-alkaline dacite and tuff.

The São Luís cratonic fragment has been considered as representing part of a Paleoproterozoic orogen (Klein et al., 2005a), with an accretionary phase (2240–2147 Ma) comprising the metavolcano-sedimentary sequence (Aurizona Group) and granitoids of the Tromaí Suite, and a collisional phase (2100–2080 Ma) represented by the peraluminous granitoids of the Tracuateua Suite and from a series of coeval granite plutons that occur as basement units in the Gurupi Belt (Fig. 1).

The Gurupi Belt is a Neoproterozoic orogen developed in the southern margin of the São Luís cratonic fragment. Most of the exposed basement of this belt is composed of reworked portions of the margin of this cratonic area (Fig. 1). These reworked rocks comprise granitoids of the Tromaí Intrusive Suite and the supracrustal Chega Tudo Formation and Gurupi Group. Other basement units are Paleoproterozoic gneisses and peraluminous granitoids, small bodies of an Archean metatonalite and a pre-orogenic body of nepheline-syenite emplaced in Neoproterozoic times (Fig. 1). Other Neoproterozoic rocks are represented by the metasedimentary rocks of the Marajupema Formation and the rounded body of the peraluminous Ney Peixoto Granite (Klein et al., 2005b).

Three small sedimentary basins, Viseu, Igarapé de Areia, and Piriá, occur over rocks of the São Luís cratonic fragment and Gurupi Belt (Fig. 1). They are composed of continental to transitional sediments and their origin, age, and tectonic meaning are still uncertain.

## 3. Granitoid types and petrography

### 3.1. Tromaí Intrusive Suite

#### 3.1.1. Cavala Tonalite

The Cavala Tonalite is composed of medium- to coarse-grained rocks having grayish to greenish colors, and equigranular to inequigranular texture. The rocks are in general massive, but they locally show a magmatic foliation. In places, when affected by narrow shear zones, they also show protomylonitic to mylonitic fabric. Centimeter- to decimeter-wide microgranular enclaves of tonalitic to dioritic composition and aggregates of mafic minerals are commonly observed.

In the QAP diagram of Streckeisen (1976) (Fig. 3), most of the modal compositions plot in similar proportions in the fields of tonalite and quartz-diorite, and subordinately in the fields of diorite, quartz-monzodiorite and granodiorite. The rocks are composed of (Table 1) plagioclase (40–55%), quartz (5–25%), and hornblende (10–35%), with minor microcline (<5%). In places, especially in quartz-diorites, relics of pyroxene are observed in the cores of amphibole crystals. Opaque minerals, such as magnetite and minor pyrite, form 2–7% of some samples. Titanite, apatite and zircon are accessory phases, whereas biotite, chlorite, calcite, white mica, and epidote occur as alteration minerals.

The quartz crystals show some evidence of solid-state deformation, such as undulose extinction and subgrain formation. Euhedral to subhedral plagioclase show some alteration to sericite, epidote and carbonate. Hornblende is dominantly anhedral, with inclusions of apatite and opaque minerals and rare pyroxene cores. In places it is altered to chlorite. The opaque minerals show commonly titanite coronas, indicating that these opaque minerals correspond to ilmenite. The granular hypidiomorphic texture is typical of the Cavala granitoids, and is characterized by the mutual contact between plagioclase and hornblende prisms, with interstitial quartz and rare microcline.

#### 3.1.2. Bom Jesus Granodiorite

The Bom Jesus Granodiorite is the predominant type of the Tromaí Intrusive Suite. The rocks are dark gray and mainly medium-grained, equigranular to porphyritic, with subordinate coarse-grained inequigranular phases. Like the Cavala granitoids, the Bom Jesus rocks are predominantly massive, with subordinate magmatic and/or tectonic foliation, and bear microgranular enclaves.

The predominant composition is granodiorite, with minor tonalite, monzogranite and rare quartz-monzodiorite (Fig. 3 and Table 1). The mineral assemblage is composed of plagioclase (40–50%), quartz (20–30%), and microcline (20%). Biotite (4–15%) is the principal mafic mineral. However, amphibole-bearing variants also occur. In these cases, hornblende occupies 15–35% of the sample volume. Biotite and hornblende do not occur in the same sample, except in cases where biotite occurs as an alteration mineral over the hornblende. Titanite, apatite, zircon, opaque minerals and rare allanite are accessory phases. White mica, chlorite, epidote and rare calcite and prehnite are alteration minerals that occur regionally.

The granitoids show granular texture, characterized by the interplay of subhedral to anhedral plagioclase and microcline prisms, with anhedral quartz grains and aggregates of mafic minerals. In the coarser-grained and porphyritic rocks, the interstices between plagioclase crystals are filled with anhedral grains of quartz, microcline and biotite. The larger plagioclase crystals, including the phenocrysts, show compositional zoning. The quartz crystals show undulose extinction, serrated contacts, and locally form aggregates. The microcline is anhedral and, in places, shows lamellae of perthite. Biotite occurs both as flakes and aggregates that are locally oriented. The hornblende form aggregates of grains with triple junctions and generally contains inclusions of quartz. The opaque minerals are anhedral and commonly show coronas of titanite.

A few occurrences of fine-grained, pink-colored monzogranites have also been found during the field work. These felsic rocks are even-grained aplites and inequigranular granophyres that indicate emplacement in shallow levels of the crust. They contain biotite and/or hornblende as mafic minerals, a characteristic that is similar to that of the Bom Jesus Granodiorite (Table 1).

### 3.1.3. Areal Granite

The Areal Granite is the less abundant type of the Tromaí Intrusive Suite, occurring as a few small stocks throughout the area (Fig. 2). The rocks show a light pink color and are normally massive, being foliated only along narrow shear zones. Fine- to coarse-grained, equigranular to inequigranular monzogranite is the predominant rock type, with subordinate occurrences of syenogranite and quartz-syenite (Fig. 3 and Table 1).

The granitoids are composed of microcline (30–50%), plagioclase (25–40%), and quartz (20–30%). Biotite is the characteristic mafic mineral, but it occurs only in small amounts (3–5%). Pyrite, magnetite, zircon, allanite, titanite, and apatite are the accessory phases. The rocks show granular texture defined by the contact of anhedral plagioclase, microcline and quartz grains. The plagioclase forms always the largest crystals that are locally zoned and with rims of myrmekite. The biotite flakes form small aggregates without preferential orientation.

## 3.2. Negra Velha Granite

The Negra Velha Granite forms two stocks of pinkish to grayish porphyritic granites that are not included in the Tromaí Intrusive Suite. Massive, porphyritic, medium- to coarse-grained monzogranites are the dominant rock types, with subordinate quartz–monzonite and syenogranite (Fig. 3 and Table 1).

These granites are composed of microcline (30–45%), plagioclase (25–35%) and quartz (20–25%). The mafic mineral is predominantly biotite and secondarily hornblende, both forming less than 10% of the total rock volume. Biotite and hornblende do not occur in association in the same sample. Titanite is the main accessory mineral that may form up to 1% of the rock volume, in addition to zircon, allanite, apatite, and opaque minerals. The Negra Velha Granite contains also very subordinate amounts of fluorite, tourmaline, rutile and possibly topaz, which is an assemblage that has not been recognized in the Tromaí granitoids.

The Negra Velha Granite show granular texture characterized by the contact of subhedral plagioclase crystals, anhedral microcline crystals with occasional perthite, and flakes of biotite or aggregates of amphibole. The mafic aggregates contain also opaque and other accessory minerals.

## 4. Geochronology

Zircon geochronology is already available for the Cavala Tonalite, Bom Jesus Granodiorite and Areal Granite of the Tromaí Intrusive Suite (Table 2 and references therein). In this paper we present new geochronological data for the Cavala Tonalite and Bom Jesus Granodiorite, using samples collected in the type locality of each granitoid type (Fig. 2), and also for the newly described Negra Velha Granite. The summary of isotopic results is presented in Tables 3 and 4, and the analytical procedures are described in Appendix A.

## 4.1. U–Pb SHRIMP results

Sample EK98 is a hornblende-bearing tonalite of the Cavala Tonalite unit. Zircon crystals are subhedral, clear and of good quality with broad igneous zoning. Eighteen crystals and 19 analyses (Table 3) conform to a simple concordant population defining a concordia age of 2159.9 ± 4.5 Ma (Fig. 4). This age is interpreted to be the crystallization age of the tonalite and is similar to the ages obtained by the Pb evaporation method (Table 2, Klein and Moura, 2001; Klein et al., 2005a), confirming the absence of inheritance in granitoids of the Cavala Tonalite.

**Table 3**
Summary of zircon U–Pb SHRIMP data of sample EK98 from the Cavala Tonalite (Tromaí Intrusive Suite)

| Zircon/spot | % $^{206}Pb_c$ | ppm U | ppm Th | $^{232}Th/^{238}U$ | ppm $^{206}Pb^*$ | (1) $^{206}Pb/^{238}U$ Age (Ma) | (1) $^{207}Pb/^{206}Pb$ Age (Ma) | % discordance | (1) $^{207}Pb^*/^{206}Pb^*$ | ±% | (1) $^{207}Pb^*/^{235}U$ | ±% | (1) $^{206}Pb^*/^{238}U$ | ±% | Errors correl |
|---|---|---|---|---|---|---|---|---|---|---|---|---|---|---|---|
| 1.1 | 0.06 | 72 | 30 | 0.43 | 25.2 | 2203 ± 26 | 2156 ± 13 | −2 | 0.1343 | 0.73 | 7.5500 | 1.6 | 0.4074 | 1.4 | 0.884 |
| 2.1 | 0.16 | 50 | 11 | 0.23 | 17.3 | 2184 ± 27 | 2141 ± 15 | −2 | 0.1333 | 0.88 | 7.4100 | 1.7 | 0.4032 | 1.4 | 0.852 |
| 3.1 | – | 88 | 35 | 0.41 | 29.8 | 2136 ± 24 | 2166 ± 11 | 1 | 0.1351 | 0.62 | 7.3200 | 1.4 | 0.3928 | 1.3 | 0.903 |
| 4.1 | 0.06 | 108 | 45 | 0.43 | 36.2 | 2128 ± 23 | 2156 ± 12 | 1 | 0.1343 | 0.71 | 7.2500 | 1.4 | 0.3911 | 1.3 | 0.871 |
| 5.1 | 0.05 | 69 | 30 | 0.44 | 23.9 | 2176 ± 26 | 2143 ± 12 | −2 | 0.1334 | 0.67 | 7.3800 | 1.5 | 0.4014 | 1.4 | 0.901 |
| 6.1 | 0.03 | 205 | 22 | 0.11 | 70.3 | 2165 ± 22 | 2155.1 ± 6.7 | 0 | 0.1343 | 0.38 | 7.3930 | 1.3 | 0.3992 | 1.2 | 0.954 |
| 6.2 | 0.04 | 93 | 36 | 0.40 | 32.7 | 2208 ± 25 | 2158 ± 10 | −2 | 0.1345 | 0.59 | 7.5800 | 1.5 | 0.4086 | 1.3 | 0.915 |
| 7.1 | 0.01 | 105 | 47 | 0.46 | 36.0 | 2161 ± 23 | 2172.5 ± 9.4 | 1 | 0.1356 | 0.54 | 7.4500 | 1.4 | 0.3984 | 1.3 | 0.920 |
| 8.1 | 0.07 | 106 | 42 | 0.41 | 36.7 | 2177 ± 23 | 2144.4 ± 9.9 | −2 | 0.1334 | 0.56 | 7.4000 | 1.4 | 0.4018 | 1.3 | 0.913 |
| 9.1 | 0.00 | 86 | 35 | 0.42 | 29.9 | 2187 ± 24 | 2145 ± 10 | −2 | 0.1335 | 0.59 | 7.4400 | 1.4 | 0.4038 | 1.3 | 0.909 |
| 10.1 | 0.05 | 132 | 53 | 0.41 | 44.8 | 2147 ± 23 | 2173.6 ± 8.8 | 1 | 0.1357 | 0.50 | 7.3970 | 1.3 | 0.3952 | 1.2 | 0.925 |
| 11.1 | 0.03 | 136 | 54 | 0.41 | 47.3 | 2195 ± 23 | 2157.7 ± 8.6 | −2 | 0.1345 | 0.49 | 7.5200 | 1.3 | 0.4056 | 1.2 | 0.929 |
| 12.1 | 0.06 | 110 | 45 | 0.43 | 37.6 | 2160 ± 23 | 2154.6 ± 9.8 | 0 | 0.1342 | 0.56 | 7.3700 | 1.4 | 0.3981 | 1.3 | 0.913 |
| 13.1 | – | 54 | 15 | 0.29 | 18.7 | 2198 ± 26 | 2174 ± 13 | −1 | 0.1358 | 0.76 | 7.6100 | 1.6 | 0.4062 | 1.4 | 0.881 |
| 14.1 | 0.07 | 52 | 16 | 0.32 | 17.6 | 2152 ± 26 | 2158 ± 14 | 0 | 0.1345 | 0.79 | 7.3500 | 1.6 | 0.3964 | 1.4 | 0.873 |
| 15.1 | 0.00 | 126 | 51 | 0.41 | 43.4 | 2166 ± 23 | 2168.3 ± 8.6 | 0 | 0.1353 | 0.49 | 7.4530 | 1.3 | 0.3994 | 1.2 | 0.929 |
| 16.1 | – | 75 | 31 | 0.43 | 25.9 | 2180 ± 29 | 2167 ± 11 | −1 | 0.1352 | 0.65 | 7.5000 | 1.7 | 0.4023 | 1.6 | 0.926 |
| 17.1 | 0.08 | 76 | 36 | 0.49 | 25.4 | 2125 ± 24 | 2156 ± 12 | 1 | 0.1343 | 0.66 | 7.2400 | 1.5 | 0.3906 | 1.3 | 0.893 |
| 18.1 | 0.00 | 53 | 12 | 0.22 | 18.2 | 2156 ± 26 | 2167 ± 13 | 1 | 0.1353 | 0.76 | 7.4100 | 1.6 | 0.3971 | 1.4 | 0.883 |

Errors are 1σ; Pbc, common Pb; Pb*, radiogenic Pb; (1) common Pb corrected using measured $^{204}Pb$.

**Table 4**
Summary of single zircon Pb evaporation results for samples from the Bom Jesus Granodiorite and Negra Velha Granite

| Zircon | $T$ (°C) | No. of ratios | $^{204}Pb/^{206}Pb$ | $2\sigma$ | $^{208}Pb/^{206}Pb$[a] | $2\sigma$ | $^{207}Pb/^{206}Pb$[a] | $2\sigma$ | Age (Ma) | 2s |
|---|---|---|---|---|---|---|---|---|---|---|
| EK147A Bom Jesus Granodiorite | | | | | | | | | | |
| 1 | 1500 | 38/38 | 0.000028 | 0.000006 | 0.12965 | 0.00165 | 0.13460 | 0.00031 | 2159 | 4 |
| 2 | 1450 | 34/34 | 0.000051 | 0.000005 | 0.17782 | 0.00040 | 0.13401 | 0.00033 | 2151 | 4 |
| | 1500 | 12/12 | 0.000056 | 0.000002 | 0.14932 | 0.00108 | 0.13386 | 0.00056 | 2149 | 7 |
| 13 | 1500 | 34/34 | 0.000093 | 0.000027 | 0.12750 | 0.00097 | 0.13387 | 0.00056 | 2149 | 7 |
| 15 | 1500 | 30/30 | 0.000039 | 0.000006 | 0.12476 | 0.00036 | 0.13515 | 0.00070 | 2166 | 9 |
| | | | | | | | | Mean | 2155 | 5 |
| EK81 Negra Velha Granite | | | | | | | | | | |
| 2 | 1500 | 0/34 | 0.000091 | 0.000008 | 0.13398 | 0.00019 | 0.13283 | 0.00018 | 2136 | 2 |
| 1 | 1500 | 36/36 | 0.000136 | 0.000020 | 0.13005 | 0.00016 | 0.12842 | 0.00018 | 2077 | 2 |
| 3 | 1500 | 36/36 | 0.000125 | 0.000003 | 0.12984 | 0.00021 | 0.12827 | 0.00021 | 2075 | 3 |
| | | | | | | | | Mean | 2076 | 2 |
| 6 | 1500 | 32/32 | 0.000169 | 0.000010 | 0.12946 | 0.00041 | 0.12703 | 0.00040 | 2058 | 6 |
| 11 | 1500 | 12/12 | 0.000177 | 0.000019 | 0.12933 | 0.00043 | 0.12667 | 0.00053 | 2053 | 7 |
| 13 | 1500 | 24/24 | 0.000198 | 0.000006 | 0.12955 | 0.00045 | 0.12687 | 0.00067 | 2056 | 9 |
| | | | | | | | | Mean | 2056 | 4 |

[a] Corrected according to Stacey and Kramers (1975).

### 4.2. Pb evaporation results

Sample EK147A is a biotite-bearing granodiorite from the Bom Jesus Granodiorite unit. Zircon grains range mostly from 0.2 to 0.3 mm in the longest dimension. They are prismatic with sharp to slightly rounded pyramids and moderately fractured. Within a population of 15 analyzed crystals 4 crystals gave suitable isotopic response and a mean age of 2155 ± 5 Ma could be calculated (Table 4). This age is similar to that of 2152 ± 3 Ma obtained in a monzogranite of the same unit by Klein and Moura (2003) (Table 2). Although, crystal 15 apparently does not belong to the same population formed by crystals 1, 2 and 13, the mean age calculated for these three crystals (2152 ± 6 Ma) still overlaps, within analytical uncertainties, with the age of zircon 15 (2166 ± 9 Ma). If they represent different populations, we may interpret the age of 2152 ± 6 Ma: (1) as the crystallization age, whereas zircon 15 represents inheritance, or (2) as reflecting Pb loss, while the age of the rock is 2166 ± 9 Ma. It is uncertain if we are really dealing with two populations. Most likely this is associate wih peculiarities of the Pb evaporation method (and mass spectrometer configuration), such as statistically precise ages (small errors) and impossibility of evaluate the degree of discordance (if any) of a zircon. Furthermore, irrespective of the chosen age (2152, 2155 or 2166 Ma), they all fall within the previously defined range of ages of the Tromaí Intrusive Suite.

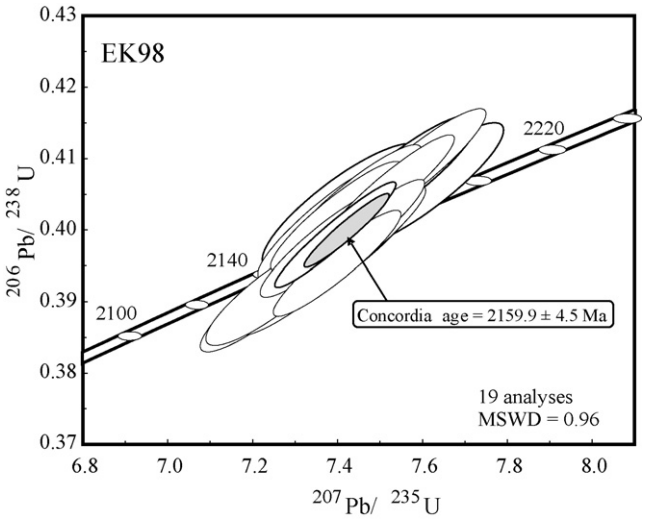


**Fig. 4.** Concordia plot for sample EK98 of the Cavala tonalite.

Sample EK81 is a biotite-bearing syenogranite of the Negra Velha Granite unit. Fourteen crystals have been analyzed and, among them, only six crystals were found to be suitable for age interpretation. These crystals gave three distinct age populations (Table 4). Grains 1 and 3 yielded a mean age of 2076 ± 2 Ma whereas grains 6, 11, and 13 furnished a mean age of 2056 ± 4 Ma. These two age populations do not overlap within analytical uncertainties. However, no significant morphological differences have been observed between zircon crystals of these two populations. The crystals have pinkish color and few inclusions, and form mostly long prisms (0.3–0.4 mm) with short sharp pyramids and concentric zoning. Finally, grain 2 is short (0.2 mm), brownish, with rather rounded pyramids, and concentric zoning. This grain gave an age of 2136 ± 2 Ma, which is interpreted as inheritance. The ages of 2076 Ma and 2056 Ma may be interpreted in two ways. (1) The value of 2076 ± 2 Ma is the age of the sample, and 2056 ± 4 Ma is related to Pb loss after crystallization; (2) the value of 2056 ± 4 Ma is the age of the sample, whereas 2076 ± 2 Ma represents inheritance, reflecting or not Pb loss. We do not have elements to define which one of the hypotheses is the correct. Nevertheless, this dating defines a magmatic event occurring at about 2056–2076 Ma, which is clearly distinct of the age of the Tromaí Intrusive Suite.

## 5. Geochemistry

The major and trace-element chemical composition of the three types of the Tromaí Intrusive Suite and of the Negra Velha Granite were determined and are presented in Table 5, and analytical procedures are described in Appendix A. A comparison between the characteristics of the different types of granitoids is shown in Table 6.

### 5.1. Tromaí Intrusive Suite

Overall, the Tromaí Intrusive Suite shows a wide range of chemical composition (Table 5), with $SiO_2$ concentration ranging from 47.5 to 75.9%, $K_2O$ content ranging from 0.3 to 4.9%, $Na_2O$ varying from 2.2 to 5.2%, and CaO varying between 0.6 and 11.5%. These data show that the Tromaí Suite is composed of low- to high-K, pre-

**Table 5a**
Chemical composition of the Cavala Tonalite (Tromaí Intrusive Suite)

| | TF7E diorite/gabbro | EK148 diorite | EK1 qz-diorite | EK98 tonalite | EK100 qz-diorite | TF24A tonalite | EK32A qz-monzodiorite | EK150A qz-diorite | EK06A tonalite |
|---|---|---|---|---|---|---|---|---|---|
| $SiO_2$ (wt.%) | 47.53 | 47.79 | 48.41 | 53.83 | 54.39 | 55.93 | 57.03 | 57.73 | 58.04 |
| $Al_2O_3$ | 16.38 | 17.37 | 16.78 | 16.08 | 15.77 | 16.43 | 17.61 | 15.91 | 17.55 |
| $Fe_2O_3$ | 14.48 | 12.10 | 9.60 | 11.00 | 10.44 | 9.98 | 8.07 | 7.95 | 6.47 |
| MgO | 3.42 | 6.03 | 7.13 | 2.89 | 2.94 | 2.85 | 2.19 | 3.37 | 2.88 |
| CaO | 8.87 | 8.95 | 11.56 | 8.07 | 7.00 | 5.62 | 6.00 | 6.91 | 5.72 |
| $Na_2O$ | 3.71 | 3.01 | 2.27 | 3.32 | 3.68 | 4.17 | 4.97 | 3.35 | 3.98 |
| $K_2O$ | 0.32 | 0.43 | 0.68 | 0.50 | 0.77 | 0.92 | 1.15 | 1.28 | 1.97 |
| $TiO_2$ | 2.48 | 0.97 | 0.79 | 1.08 | 2.08 | 0.92 | 0.88 | 0.92 | 0.63 |
| $P_2O_5$ | 1.26 | 0.40 | 0.20 | 0.62 | 0.89 | 0.4 | 0.46 | 0.32 | 0.31 |
| MnO | 0.32 | 0.17 | 0.15 | 0.19 | 0.22 | 0.31 | 0.21 | 0.13 | 0.12 |
| $Cr_2O_3$ | 0.001 | 0.01 | 0.034 | 0.003 | 0.002 | 0.001 | 0.001 | 0.008 | 0.002 |
| LOI | 1.0 | 2.7 | 2.2 | 2.3 | 1.7 | 2.2 | 1.3 | 2.0 | 2.2 |
| Total | 99.78 | 99.93 | 99.81 | 99.89 | 99.89 | 99.73 | 99.87 | 99.88 | 99.87 |
| Ba (ppm) | 202 | 232 | 269 | 302 | 428 | 608 | 618 | 520 | 792 |
| Cs | 0.3 | 0.2 | 0.2 | <0.1 | 0.2 | 0.4 | 0.3 | 0.5 | 0.9 |
| Ga | 21.1 | 20.9 | 15.7 | 21.8 | 19.3 | 20 | 19.4 | 17.4 | 18.3 |
| Hf | 0.9 | 1.4 | 0.8 | 1.6 | 2.4 | 2.6 | 1.2 | 4.0 | 2.1 |
| Nb | 4.5 | 3.1 | 1.3 | 3.5 | 5.2 | 4.0 | 3.7 | 6.9 | 4.8 |
| Rb | 4 | 6 | 11 | 10 | 14 | 17 | 21 | 35 | 48 |
| Sr | 548 | 695 | 495 | 755 | 596 | 606 | 630 | 567 | 641 |
| Ta | 0.3 | <0.1 | 0.1 | 0.3 | 0.3 | 0.2 | 0.2 | 0.3 | 0.2 |
| Th | <0.1 | 0.3 | 0.8 | 1.1 | 1.0 | 1.9 | 0.9 | 0.9 | 1.9 |
| U | 0.1 | <0.1 | 0.4 | 0.7 | 0.5 | 0.6 | 0.5 | 0.4 | 0.5 |
| Sc | 39 | 29 | 38 | 25 | 28 | 24 | 21 | 24 | 15 |
| V | 75 | 252 | 223 | 144 | 71 | 99 | 72 | 162 | 109 |
| Zr | 32 | 28 | 33 | 63 | 88 | 83 | 33 | 150 | 69 |
| Y | 42 | 27 | 11 | 46 | 36 | 39 | 42 | 32 | 20 |
| Cu | 23.2 | 7.5 | 23.9 | 39.1 | 17.1 | 25.5 | 20.7 | 56.5 | 36.7 |
| Pb | 0.6 | 0.7 | 1.3 | 1.4 | 1.1 | 1.6 | 1.1 | 1.3 | 1.8 |
| Zn | 109 | 59 | 25 | 95 | 72 | 140 | 77 | 50 | 44 |
| Ni | 7.5 | 17.4 | 11.7 | 10.6 | 4 | 8.3 | 3 | 14 | 10.1 |
| La | 18.5 | 12.4 | 11.2 | 19.5 | 17.9 | 17.6 | 18 | 18.3 | 16.6 |
| Ce | 46.9 | 35.3 | 20.9 | 45.1 | 44.8 | 45.1 | 48.6 | 47 | 40.4 |
| Pr | 6.88 | 5.27 | 3.51 | 5.99 | 6.04 | 6.13 | 6.49 | 6.47 | 5.2 |
| Nd | 33.3 | 24.2 | 16.4 | 27.7 | 27.6 | 32 | 31.7 | 29.6 | 22.1 |
| Sm | 7.9 | 5.9 | 3.2 | 7.7 | 6.4 | 6.8 | 6.8 | 6.6 | 4.4 |
| Eu | 3.27 | 1.71 | 1.05 | 2.64 | 2.5 | 2.4 | 2.31 | 1.47 | 1.14 |
| Gd | 8.24 | 4.93 | 2.4 | 7.93 | 7.08 | 6.66 | 7.15 | 5.5 | 3.48 |
| Tb | 1.37 | 0.83 | 0.36 | 1.27 | 1.12 | 1.25 | 1.31 | 0.94 | 0.54 |
| Dy | 7.19 | 4.12 | 2.14 | 7.06 | 5.84 | 6.29 | 6.9 | 4.76 | 2.88 |
| Ho | 1.42 | 0.86 | 0.45 | 1.61 | 1.29 | 1.36 | 1.43 | 0.97 | 0.65 |
| Er | 4.33 | 2.64 | 1.21 | 4.59 | 3.52 | 3.76 | 4.26 | 2.97 | 1.71 |
| Tm | 0.63 | 0.35 | 0.22 | 0.67 | 0.5 | 0.56 | 0.65 | 0.44 | 0.25 |
| Yb | 3.55 | 2.28 | 0.95 | 4.11 | 3.36 | 3.72 | 4.08 | 2.73 | 1.5 |
| Lu | 0.47 | 0.34 | 0.13 | 0.6 | 0.46 | 0.51 | 0.56 | 0.44 | 0.21 |
| Σ REE | 144 | 101 | 64 | 136 | 128 | 134 | 140 | 128 | 101 |
| Eu/Eu* | 1.2 | 1.0 | 1.2 | 1.0 | 1.1 | 1.1 | 1.0 | 0.7 | 0.9 |
| LaN/YbN | 3.5 | 3.7 | 7.9 | 3.2 | 3.6 | 3.2 | 3.0 | 4.5 | 7.5 |
| LaN/SmN | 1.47 | 1.32 | 2.20 | 1.59 | 1.76 | 1.63 | 1.67 | 1.74 | 2.37 |
| CeN/YbN | 2.62 | 2.13 | 3.14 | 1.83 | 2.12 | 1.83 | 1.61 | 1.53 | 2.16 |
| CeN/SmN | 3.42 | 4.00 | 5.69 | 2.84 | 3.45 | 3.14 | 3.08 | 4.45 | 6.97 |
| EuN/YbN | 1.43 | 1.44 | 1.58 | 1.41 | 1.69 | 1.60 | 1.72 | 1.72 | 2.22 |
| Fe + Mg + Ti | 20.38 | 19.10 | 17.52 | 14.97 | 15.46 | 13.75 | 11.14 | 12.24 | 9.98 |
| Ba/Rb | 53.16 | 38.02 | 23.82 | 29.93 | 29.71 | 34.95 | 29.72 | 14.78 | 16.64 |
| Rb/Sr | 0.01 | 0.01 | 0.02 | 0.01 | 0.02 | 0.03 | 0.03 | 0.06 | 0.07 |
| Sr/Ba | 2.71 | 3.00 | 1.84 | 2.50 | 1.39 | 1.00 | 1.02 | 1.09 | 0.81 |
| Rb/Zr | 0.12 | 0.22 | 0.34 | 0.16 | 0.16 | 0.21 | 0.63 | 0.23 | 0.69 |
| Sr/Y | 13.14 | 25.76 | 45.01 | 16.38 | 16.46 | 15.69 | 15.18 | 17.83 | 32.89 |
| Ba/La | 10.92 | 18.70 | 24.04 | 15.50 | 23.90 | 34.56 | 34.34 | 28.42 | 47.72 |
| Sm/Yb | 2.23 | 2.59 | 3.37 | 1.87 | 1.90 | 1.83 | 1.67 | 2.42 | 2.93 |
| La/Sm | 2.34 | 2.10 | 3.50 | 2.53 | 2.80 | 2.59 | 2.65 | 2.77 | 3.77 |

LOI: loss on ignition.

dominantly medium-K, rocks, according to Peccerillo and Taylor (1976) (Fig. 5A), or high-K calc-alkaline rocks if the proposal of Nardi et al. (2005) is used (Fig. 5B). The suite is also composed of metaluminous to weakly peraluminous granitoids (Fig. 5C). In terms of K–Na–Ca relationships the samples follow predominantly a granodioritic trend (Fig. 6A); they plot in the calcic–alkalic and subordinately calcic fields of the diagram of Frost et al. (2001) (Fig. 6B); and scatter along a Na-enriched calc-alkaline trend in the diagram of Barker and Arth (1976) (Fig. 6C). This latter feature is probably the reason why Klein et al. (2005a) observed characteristics of both calc-alkaline and TTG granitoids in the chemical data presented by Pastana (1995). Post-magmatic (hydrothermal)

**Table 5b**
Chemical composition of the Bom Jesus Granodiorite (Tromaí Intrusive Suite) and of shallow intrusions (*)

| | EK167A granodiorite | EK25 tonalite | TF12 tonalite | EK164A granodiorite | EK189 tonalite | EK188 tonalite | EK142A granodiorite | EK147A granodiorite | EK19A monzogranite | EK163* monzogranite | EK30* aplite |
|---|---|---|---|---|---|---|---|---|---|---|---|
| $SiO_2$ (wt.%) | 62.06 | 64.56 | 66.5 | 67.51 | 67.7 | 68.49 | 68.99 | 69.26 | 69.7 | 70.6 | 72.01 |
| $Al_2O_3$ | 15.08 | 14.85 | 16.56 | 15.33 | 15.44 | 14.96 | 14.68 | 14.45 | 15.08 | 13.53 | 13.35 |
| $Fe_2O_3$ | 8.06 | 4.37 | 3.38 | 3.50 | 3.43 | 3.42 | 3.73 | 3.85 | 2.61 | 4.45 | 4.09 |
| MgO | 1.88 | 1.75 | 1.14 | 1.20 | 1.14 | 1.06 | 0.92 | 0.90 | 0.85 | 0.69 | 0.23 |
| CaO | 5.21 | 4.1 | 4.04 | 3.47 | 2.52 | 2.72 | 2.99 | 3.07 | 2.51 | 2.12 | 1.72 |
| $Na_2O$ | 3.82 | 3.83 | 4.90 | 3.97 | 5.20 | 3.31 | 4.17 | 4.20 | 3.80 | 4.67 | 4.41 |
| $K_2O$ | 0.70 | 2.57 | 1.53 | 2.72 | 1.92 | 3.96 | 2.70 | 2.31 | 3.82 | 2.72 | 3.06 |
| $TiO_2$ | 0.94 | 0.59 | 0.51 | 0.46 | 0.41 | 0.44 | 0.44 | 0.47 | 0.36 | 0.46 | 0.37 |
| $P_2O_5$ | 0.29 | 0.15 | 0.23 | 0.15 | 0.15 | 0.13 | 0.16 | 0.15 | 0.12 | 0.12 | 0.06 |
| MnO | 0.14 | 0.07 | 0.06 | 0.06 | 0.05 | 0.04 | 0.08 | 0.09 | 0.05 | 0.07 | 0.07 |
| $Cr_2O_3$ | 0.003 | 0.003 | 0.002 | 0.002 | 0.001 | 0.004 | 0.001 | 0.002 | 0.004 | 0.001 | 0.001 |
| LOI | 1.7 | 3.1 | 1.0 | 1.5 | 2.0 | 1.4 | 1.0 | 1.1 | 1.1 | 0.5 | 0.5 |
| Total | 99.88 | 99.95 | 99.85 | 99.87 | 99.96 | 99.93 | 99.87 | 99.85 | 100 | 99.93 | 99.87 |
| Ba | 670 | 684 | 630 | 823 | 681 | 1325 | 875 | 888 | 727 | 1087 | 1115 |
| Cs | 0.3 | 1.3 | 0.6 | 1.4 | 1.0 | 1.1 | 1.0 | 0.4 | 2.5 | 0.6 | 0.6 |
| Ga | 17.9 | 16.9 | 19 | 15 | 20.3 | 16.1 | 15.5 | 16.2 | 16.7 | 16.8 | 16.7 |
| Hf | 5.2 | 3.3 | 2.2 | 3.4 | 3.7 | 6.1 | 3.9 | 5.8 | 4.4 | 5.8 | 6.4 |
| Nb | 7.2 | 5.2 | 7 | 5.9 | 5 | 5.8 | 4.6 | 5.4 | 5.9 | 6.6 | 7.9 |
| Rb | 11 | 67 | 28 | 61 | 52 | 105 | 56 | 43 | 128 | 55 | 50 |
| Sr | 446 | 533 | 958 | 468 | 632 | 480 | 369 | 371 | 388 | 237 | 270 |
| Ta | 0.5 | 0.6 | 0.6 | 0.5 | 0.2 | 0.5 | 0.3 | 0.3 | 0.6 | 0.5 | 0.6 |
| Th | 2 | 5.6 | 1.6 | 4.7 | 6.2 | 4.7 | 2.9 | 1.6 | 10.5 | 3.5 | 2.1 |
| U | 1.0 | 1.0 | 0.4 | 1.9 | 2.6 | 1.5 | 0.7 | 0.7 | 4.3 | 1.4 | 0.6 |
| Sc | 18 | 9 | 8 | 8 | 5 | 7 | 9 | 9 | 6 | 11 | 12 |
| V | 65 | 97 | 44 | 43 | 42 | 54 | 35 | 37 | 40 | 22 | <5 |
| Zr | 177 | 116 | 86 | 111 | 133 | 219 | 159 | 155 | 147 | 198 | 204 |
| Y | 37 | 14 | 10 | 17 | 7 | 19 | 24 | 30 | 13 | 63 | 36 |
| Cu | 28.7 | 53.6 | 18.2 | 17.2 | 12.0 | 13.5 | 22.1 | 31.7 | 26.4 | 26 | 10.5 |
| Pb | 2.0 | 12.7 | 2.0 | 2.9 | 5.3 | 1.8 | 2.7 | 2.3 | 4.3 | 7.4 | 1.8 |
| Zn | 77 | 35 | 51 | 48 | 42 | 33 | 60 | 45 | 29 | 38 | 22 |
| Ni | 9.9 | 11.5 | 7.3 | 9.9 | 6.3 | 9.5 | 3.8 | 4.7 | 7.8 | 2.4 | 1.5 |
| La | 20.8 | 26.0 | 12.7 | 16.1 | 17.5 | 32.2 | 24.3 | 19.6 | 24.1 | 37.3 | 26.2 |
| Ce | 46.2 | 50.4 | 34.1 | 37.9 | 37.1 | 69.7 | 48.9 | 42.6 | 49.8 | 69.8 | 57.3 |
| Pr | 6.08 | 5.25 | 4.51 | 4.49 | 3.91 | 7.46 | 5.69 | 5.42 | 5.19 | 9.86 | 7.73 |
| Nd | 25.9 | 20.5 | 21.9 | 17 | 15.5 | 28 | 23.4 | 22.9 | 18.5 | 43.2 | 36.2 |
| Sm | 6.6 | 3.5 | 3.9 | 4.2 | 2.7 | 4.8 | 4.3 | 4.9 | 3.2 | 9.0 | 8.0 |
| Eu | 1.84 | 0.98 | 0.99 | 0.91 | 0.87 | 1.01 | 1.1 | 1.27 | 0.75 | 2.07 | 1.76 |
| Gd | 5.7 | 2.81 | 2.63 | 2.81 | 1.79 | 3.47 | 3.88 | 4.58 | 2.28 | 9.19 | 6.91 |
| Tb | 1.04 | 0.36 | 0.37 | 0.51 | 0.22 | 0.58 | 0.71 | 0.71 | 0.37 | 1.48 | 1.16 |
| Dy | 5.72 | 2.17 | 1.59 | 2.51 | 1.17 | 3.3 | 3.78 | 4.28 | 1.96 | 9.81 | 6.99 |
| Ho | 1.23 | 0.40 | 0.32 | 0.54 | 0.18 | 0.62 | 0.79 | 0.95 | 0.39 | 1.90 | 1.38 |
| Er | 3.93 | 1.12 | 0.89 | 1.78 | 0.59 | 1.77 | 2.45 | 3.05 | 1.22 | 5.71 | 4.01 |
| Tm | 0.56 | 0.18 | 0.13 | 0.25 | 0.08 | 0.3 | 0.36 | 0.48 | 0.18 | 0.83 | 0.71 |
| Yb | 3.98 | 1.06 | 1.28 | 1.39 | 0.66 | 1.71 | 2.39 | 2.83 | 1.3 | 5.56 | 4.56 |
| Lu | 0.58 | 0.17 | 0.13 | 0.26 | 0.09 | 0.25 | 0.36 | 0.43 | 0.21 | 0.80 | 0.59 |
| Σ REE | 130 | 115 | 85 | 91 | 82 | 155 | 122 | 114 | 109 | 207 | 164 |
| Eu/Eu* | 0.9 | 1.0 | 0.9 | 0.8 | 1.2 | 0.8 | 0.8 | 0.8 | 0.8 | 0.7 | 0.7 |
| LaN/YbN | 3.5 | 16.5 | 6.7 | 7.8 | 17.9 | 12.7 | 6.9 | 4.7 | 12.5 | 4.5 | 3.9 |
| LaN/SmN | 1.98 | 4.67 | 2.05 | 2.41 | 4.08 | 4.22 | 3.55 | 2.52 | 4.74 | 2.61 | 2.06 |
| CeN/YbN | 1.31 | 2.63 | 2.20 | 1.86 | 3.75 | 1.68 | 1.31 | 1.28 | 1.64 | 1.06 | 1.10 |
| CeN/SmN | 3.00 | 12.30 | 6.89 | 7.05 | 14.54 | 10.54 | 5.29 | 3.89 | 9.91 | 3.25 | 3.25 |
| EuN/YbN | 1.69 | 3.48 | 2.11 | 2.18 | 3.32 | 3.50 | 2.74 | 2.10 | 3.76 | 1.87 | 1.73 |
| Fe + Mg + Ti | 10.88 | 6.71 | 5.03 | 5.16 | 4.98 | 4.92 | 5.09 | 5.22 | 3.82 | 5.60 | 4.69 |
| Ba/Rb | 61.50 | 10.18 | 22.34 | 13.45 | 13.06 | 12.62 | 15.77 | 20.83 | 5.66 | 19.79 | 22.11 |
| Rb/Sr | 0.02 | 0.13 | 0.03 | 0.13 | 0.08 | 0.22 | 0.15 | 0.11 | 0.33 | 0.23 | 0.19 |
| Sr/Ba | 0.67 | 0.78 | 1.52 | 0.57 | 0.93 | 0.36 | 0.42 | 0.42 | 0.53 | 0.22 | 0.24 |
| Rb/Zr | 0.06 | 0.58 | 0.33 | 0.55 | 0.39 | 0.48 | 0.35 | 0.27 | 0.87 | 0.28 | 0.25 |
| Sr/Y | 12.22 | 39.15 | 92.08 | 27.99 | 91.64 | 25.12 | 15.25 | 12.41 | 30.09 | 3.77 | 7.48 |
| Ba/La | 32.23 | 26.31 | 49.60 | 51.13 | 38.89 | 41.16 | 36.02 | 45.28 | 30.15 | 29.13 | 42.54 |
| Sm/Yb | 1.66 | 3.30 | 3.05 | 3.02 | 4.09 | 2.81 | 1.80 | 1.73 | 2.46 | 1.62 | 1.75 |
| La/Sm | 3.15 | 7.43 | 3.26 | 3.83 | 6.48 | 6.71 | 5.65 | 4.00 | 7.53 | 4.14 | 3.28 |

LOI: loss on ignition.

alteration is observed in samples of the Cavala and Bom Jesus units (LOI up to 2.7%) and to a lesser extent in the Areal Granite, which is a consequence of the development of sericite and epidote over plagioclase and of chlorite over amphibole and/or biotite.

*5.1.1. Cavala Tonalite*

The Cavala Tonalite shows the largest compositional variation among the studied granitoids, with $SiO_2$ content between 47 and 58%, and $K_2O$ content ranging from 0.3 to 2.0%. The sum of $Fe_2O_3 + MgO + TiO_2$, elements that are typical of the ferromag-

**Table 5c**
Chemical composition of the Areal Granite (Tromaí Intrusive Suite) and Negra Velha Granite

| | Areal granite | | | | Negra Velha Granite | | |
|---|---|---|---|---|---|---|---|
| | EK190 monzogranite | EK178 monzogranite | EK162 syenogranite | EK33 syenogranite | EK20 qz-monzonite | EK15 monzogranite | EK81 syenogranite |
| $SiO_2$ (wt.%) | 73.42 | 74.04 | 75.3 | 75.9 | 66.58 | 68.85 | 70.41 |
| $Al_2O_3$ | 13.31 | 14.37 | 13.16 | 13.23 | 16.00 | 15.22 | 15.45 |
| $Fe_2O_3$ | 2.07 | 0.99 | 1.30 | 1.23 | 2.22 | 1.96 | 1.39 |
| MgO | 0.42 | 0.21 | 0.19 | 0.13 | 0.98 | 0.75 | 0.47 |
| CaO | 1.16 | 0.94 | 0.83 | 0.64 | 1.66 | 1.61 | 1.55 |
| $Na_2O$ | 3.84 | 4.08 | 3.69 | 3.99 | 5.02 | 4.99 | 4.91 |
| $K_2O$ | 3.76 | 4.85 | 4.69 | 4.14 | 5.38 | 4.94 | 4.56 |
| $TiO_2$ | 0.24 | 0.11 | 0.14 | 0.12 | 0.33 | 0.31 | 0.29 |
| $P_2O_5$ | 0.06 | 0.04 | 0.03 | 0.02 | 0.20 | 0.20 | 0.16 |
| MnO | 0.05 | 0.06 | 0.02 | 0.03 | 0.05 | 0.03 | 0.02 |
| $Cr_2O_3$ | 0.001 | 0.001 | 0.001 | 0.001 | 0.005 | 0.003 | 0.002 |
| LOI | 1.7 | 0.4 | 0.6 | 0.5 | 1.2 | 0.7 | 0.5 |
| Total | 100.03 | 100.08 | 99.96 | 99.93 | 99.63 | 99.56 | 99.72 |
| Ba (ppm) | 955 | 710 | 545 | 845 | 2314 | 1260 | 1385 |
| Cs | 1.1 | 4.1 | 0.9 | 1.3 | 4.6 | 4.9 | 11 |
| Ga | 14.6 | 15.6 | 12.7 | 11.4 | 19.1 | 19.5 | 21.7 |
| Hf | 4.9 | 2.5 | 3.7 | 3.7 | 8.3 | 10.0 | 6.0 |
| Nb | 6.8 | 9.7 | 5.2 | 6.2 | 12.5 | 13.4 | 7.3 |
| Rb | 102 | 188 | 136 | 137 | 149 | 201 | 166 |
| Sr | 244 | 138 | 96 | 98 | 1608 | 1075 | 1084 |
| Ta | 0.6 | 1.1 | 0.7 | 0.5 | 0.9 | 1.1 | 0.6 |
| Th | 9.1 | 9.0 | 9.2 | 10.0 | 24.6 | 28.5 | 10.8 |
| U | 2.6 | 3.0 | 3.1 | 3.2 | 5.8 | 12.8 | 12.1 |
| Sc | 3 | 3 | 2 | 2 | 3 | 2 | 3 |
| V | 13 | 6 | 7 | <5 | 27 | 22 | 17 |
| Zr | 138 | 67 | 107 | 94 | 315 | 314 | 165 |
| Y | 23 | 46 | 29 | 21 | 33 | 12 | 6 |
| Cu | 7.0 | 17.8 | 19.4 | 5.7 | 22.4 | 6.5 | 27.7 |
| Pb | 4.3 | 8.0 | 6.6 | 4.4 | 29.9 | 43.3 | 11.2 |
| Zn | 17 | 25 | 19 | 13 | 40 | 33 | 32 |
| Ni | 3.8 | 1.7 | 3.6 | 3.3 | 15.4 | 10.7 | 9.1 |
| La | 28.7 | 21.4 | 42.5 | 30.8 | 159.7 | 81.8 | 38.4 |
| Ce | 60.2 | 43.6 | 85.5 | 68 | 219.3 | 152.8 | 86.9 |
| Pr | 6.55 | 5.23 | 9.32 | 7.76 | 31.17 | 16.25 | 9.07 |
| Nd | 24.1 | 20.7 | 34.7 | 29.6 | 111.3 | 55.3 | 32.8 |
| Sm | 4.1 | 5.1 | 5.6 | 4.1 | 17.3 | 7.7 | 5.8 |
| Eu | 0.55 | 0.53 | 0.43 | 0.39 | 4.53 | 1.93 | 1.44 |
| Gd | 3.07 | 5.37 | 3.72 | 3.31 | 11.35 | 4.11 | 3.09 |
| Tb | 0.55 | 0.98 | 0.73 | 0.59 | 1.26 | 0.6 | 0.39 |
| Dy | 3.53 | 6.62 | 3.55 | 2.9 | 6.02 | 2.52 | 1.53 |
| Ho | 0.67 | 1.36 | 0.79 | 0.69 | 0.84 | 0.36 | 0.2 |
| Er | 2.18 | 4.14 | 2.38 | 2.09 | 2.01 | 0.89 | 0.55 |
| Tm | 0.33 | 0.63 | 0.33 | 0.39 | 0.26 | 0.18 | 0.06 |
| Yb | 2.37 | 4.17 | 2.65 | 2.37 | 1.45 | 1.12 | 0.35 |
| Lu | 0.34 | 0.57 | 0.42 | 0.33 | 0.2 | 0.15 | 0.06 |
| Σ REE | 137 | 120 | 193 | 153 | 567 | 326 | 181 |
| Eu/Eu* | 0.5 | 0.3 | 0.3 | 0.3 | 1.0 | 1.0 | 1.0 |
| LaN/YbN | 8.2 | 3.5 | 10.8 | 8.8 | 74.3 | 49.2 | 74.0 |
| LaN/SmN | 4.40 | 2.64 | 4.77 | 4.73 | 5.81 | 6.68 | 4.16 |
| CeN/YbN | 0.66 | 0.36 | 0.46 | 0.47 | 8.88 | 4.90 | 11.70 |
| CeN/SmN | 6.57 | 2.70 | 8.35 | 7.42 | 39.12 | 35.29 | 64.22 |
| EuN/YbN | 3.54 | 2.06 | 3.68 | 4.00 | 3.06 | 4.79 | 3.62 |
| Fe + Mg + Ti | 2.73 | 1.31 | 1.63 | 1.48 | 3.53 | 3.02 | 2.15 |
| Ba/Rb | 9.34 | 3.78 | 4.01 | 6.16 | 15.50 | 6.27 | 8.36 |
| Rb/Sr | 0.42 | 1.36 | 1.42 | 1.39 | 0.09 | 0.19 | 0.15 |
| Sr/Ba | 0.26 | 0.19 | 0.18 | 0.12 | 0.69 | 0.85 | 0.78 |
| Rb/Zr | 0.74 | 2.79 | 1.27 | 1.46 | 0.47 | 0.64 | 1.00 |
| Sr/Y | 10.80 | 3.03 | 3.27 | 4.69 | 48.43 | 92.65 | 169.41 |
| Ba/La | 33.27 | 33.15 | 12.83 | 27.44 | 14.49 | 15.41 | 36.06 |
| Sm/Yb | 1.73 | 1.22 | 2.11 | 1.73 | 11.93 | 6.88 | 16.57 |
| La/Sm | 7.00 | 4.20 | 7.59 | 7.51 | 9.23 | 10.62 | 6.62 |

LOI: loss on ignition.

nesian minerals, ranges from 10.0 to 20.4%, and the $K_2O/Na_2O$ ratios are quite lower than one (Tables 5 and 6). The Cavala granitoids are low- to medium-K metaluminous rocks, which is consistent with the presence of amphibole as the unique mafic mineral.

The trace-element data show the highest Sc and V concentrations among the studied granitoids. The Rb/Sr and Rb/Zr ratios are very low (<0.07 and 0.12–0.69, respectively), whereas other ratios of petrogenetic importance are very variable (Table 5a): Ba/La = 11–48, Sr/Y = 13–45, La/Yb(n) 3–8. The primitive mantle-

**Table 6**
Comparison between granitoids of the Tromaí Intrusive Suíte and the Negra Velha Granite

| | Tromaí Intrusive Suite | | | Negra Velha Granite |
|---|---|---|---|---|
| | Cavala Tonalite | Bom Jesus Granodiorite | Areal Granite | |
| Petrographic types (QAP) | Tonalite, quartz-diorite, diorite, quartz-monzodiorite | Granodiorite, tonalite, quartz-monzodiorite, monzogranite | Monzogranite, syenogranite, quartz-syenite | Syenogranite, monzogranite, quartz-monzonite |
| Normative types | Tonalite | Granodiorite (tonalite, quartz-monzonite) | Granite | Granite |
| Mafic mineralogy | Amphibole (pyroxene) | Biotite (rare amphibole) | Biotite | Biotite (amphibole) |
| Accessory mineralogy | Titanite, apatite, zircon | Titanite, apatite, allanite, zircon | Titanite, allanite, apatite, zircon | titanite, zircon (tourmaline, fluorite) |
| Texture | Medium- to coarse-grained, equigranular, inequigranular | Coarse-grained inequigranular porphyritic (equigranular) | Fine-grained equigranular and inequigranular to coarse-grained porphyritic | Medium- to coarse-grained, porphyritic |
| $SiO_2$ (wt%) | 47–58 | 62–70 | 73–76 | 66–70 |
| $K_2O/Na_2O$ | $\ll 1$ | <1 | >1 | ~1 |
| Alumina saturation index | Strongly metaluminous | Weakly metaluminous to peraluminous | Weakly peraluminous | Weakly metaluminous |
| $K_2O$ content | Low to moderate | moderate (high) | High | High |
| $Fe_2O_3 + MgO + TiO_2$ (wt%) | 10–20 | 5–11 | 1–3 | 2–4 |
| Rb (ppm) | 4–48 | 11–128 | 102–188 | 149–201 |
| Sr | 495–755 | 369–958 | 96–244 | 1075–1608 |
| Ba | 202–792 | 630–888(1325) | 545–955 | 1260-2314 |
| Zr (ppm) | 28–150 | 86–219 | 67–138 | 165–315 |
| Y | 11–49 | 7–37 | 21–46 | 6–33 |
| Nb | 1.3–6.9 | 4.6–7.2 | 5.2–9.7 | 7.3–13.4 |
| ΣREE (ppm) | 64–144 | 85–155 | 120–193 | 181–567 |
| La/Yb(n) | 3–8 | 3–18 | 3–11 | 49–74 |
| Eu/Eu[a] | 0.7–1.2 | 0.8–1.2 | 0.3–0.5 | 1.0 |
| Ba/La | 11–48 | 26–51 | 13–33 | 14–36 |
| Sr/Y | 13–45 | 12–92 | 3–11 | 48–169 |
| Rb/Sr | 0.007–0.074 | 0.024–0.331 | 0.419–1.415 | 0.093–0.187 |
| Ni (ppm) | 3.0–17.4 | 4.7–11.5 | 1.7–3.8 | 9.1–15.4 |
| V | 71–252 | 35–97 | 5–13 | 17–27 |
| Sc | 15–39 | 6–18 | 2–3 | 2–3 |
| Hf | 0.8–4.0 | 2.2–6.1 | 2.5–4.9 | 6.0–10.0 |
| AFM | Tholeiitic, calc-alkaline | Calc-alkaline | Calc-alkaline | Calc-alkaline |
| Age (Ma) | 2168 ± 4 to 2160 ± 2 | 2152 ± 3 | 2163 ± 3 to 2149 ± 4 | 2076 ± 2 to 2056 ± 4 |
| $T_{DM}$ (Ga) | 2.26 | 1.23 | 2.26 | na[a] |
| εNd(t) | +2.2 | +2.3 | +1.9 | na |

[a] na: not available.

normalized multi-element diagram (Fig. 7A) shows enrichment in large ion litophile (LIL) elements in relation to the high field strength (HFS) elements, in addition to sharp negative anomalies of Nb, Zr, and Ti. The rare earth elements (REE) contents vary between 64 ppm and 144 ppm and show weak fractionation of light REE in relation to heavy REE (Fig. 7B), and absence of Eu anomaly ($Eu/Eu^* = 0.7–1.2$).

Within the Cavala unit, some differences are observed between the more primitive samples, with $SiO_2$ content lower than 50%, and those samples with $SiO_2$ content higher than 54% (Table 5a). The more primitive samples (and to some extent sample EK98) have higher concentrations of $Fe_2O_3$, CaO, Sc and a higher Sr/Y ratio, and lower contents of $K_2O$, Ba, Rb, and also a lower Ba/La ratio, when compared to the other samples.

### 5.1.2. Bom Jesus Granodiorite

The Bom Jesus Granodiorite has $SiO_2$ concentrations between 62.0 and 69.7% and $K_2O$ between 0.7 and 4.0%, which characterizes this sequence as composed of medium- to subordinately high-K rocks (Fig. 5A). The sum of $Fe_2O_3 + MgO + TiO_2$ varies from 5.0 to 10.9%, and the $K_2O/Na_2O$ ratios are lower than one (Table 5b). Regarding the alumina saturation index, the samples of the Bom Jesus Granodiorite plot in both sides of the limit between the metaluminous and peraluminous fields (Fig. 5B). This is in keeping with the presence of biotite and subordinate amphibole in the mineral assemblage.

The trace-elements do not show a characteristic pattern. In general they show intermediate values between those of the more primitive Cavala Tonalite and the more evolved Areal Granite. However, one can observe a larger variation between the maximum and minimum values, when compared to the other granitoid types (Tables 5 and 6). As observed in the Cavala type, the Rb/Sr (<0.33) and Rb/Zr (<0.87) ratios are also low.

The extended multi-element normalized diagram (Fig. 7C) shows an enrichment of LIL elements in relation to the HFS elements, with negative Nb, P, and Ti anomalies. This pattern differs slightly from that of the Cavala by the positive Ce and Pb anomalies and absence of the negative Zr break in the Bom Jesus samples. The REE contents vary between 85 ppm and 155 ppm and are slightly higher than those of the Cavala Tonalite and slightly lower than that presented by the Areal Granite. The REE pattern is characterized by a weak fractionation between the light and heavy REE, with La/Yb(n) ratio between 3 and 18 and absence of Eu anomaly ($Eu/Eu^* = 0.8–1.2$). The heavy REE show a flatter distribution in relation to that of the Cavala Tonalite (Fig. 7B and D).

Two samples of aplite and granophyre have $SiO_2$ contents of 72.0 and 70.6%, and $K_2O$ of 3.1 and 2.7%, respectively (Table 5b). These fine-grained monzogranites normally plot in intermediate positions between the samples of the Bom Jesus and Areal units in the geochemical diagrams. The REE contents, however, are higher and the fractionation between light and heavy REE is smaller than those of the Bom Jesus Granodiorite, and negative Eu anomaly is

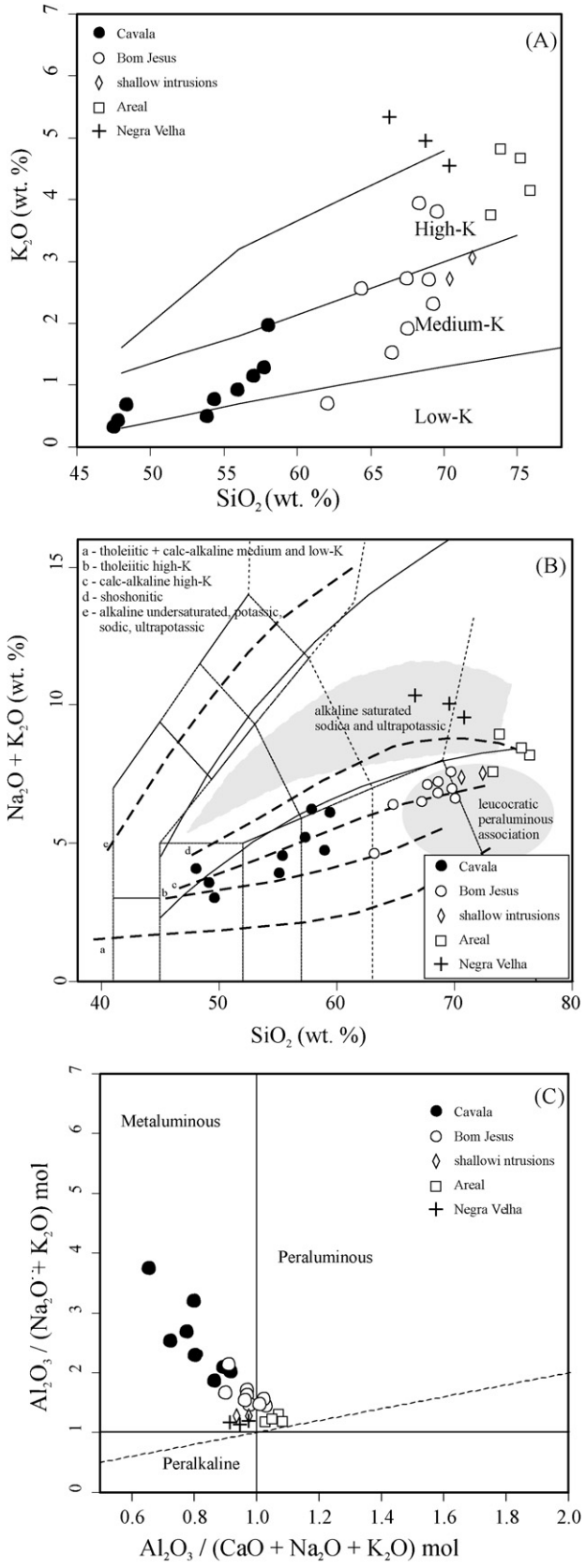


**Fig. 5.** (A) $SiO_2$ versus $K_2O$ (Peccerillo and Taylor, 1976), (B) $SiO_2$ versus $K_2O + Na_2O$ (Nardi et al., 2005), and (C) A/NK versus A/CKN (Shand diagram) plots for the granitoids of the Tromaí Intrusive Suite and Negra Velha Granite.

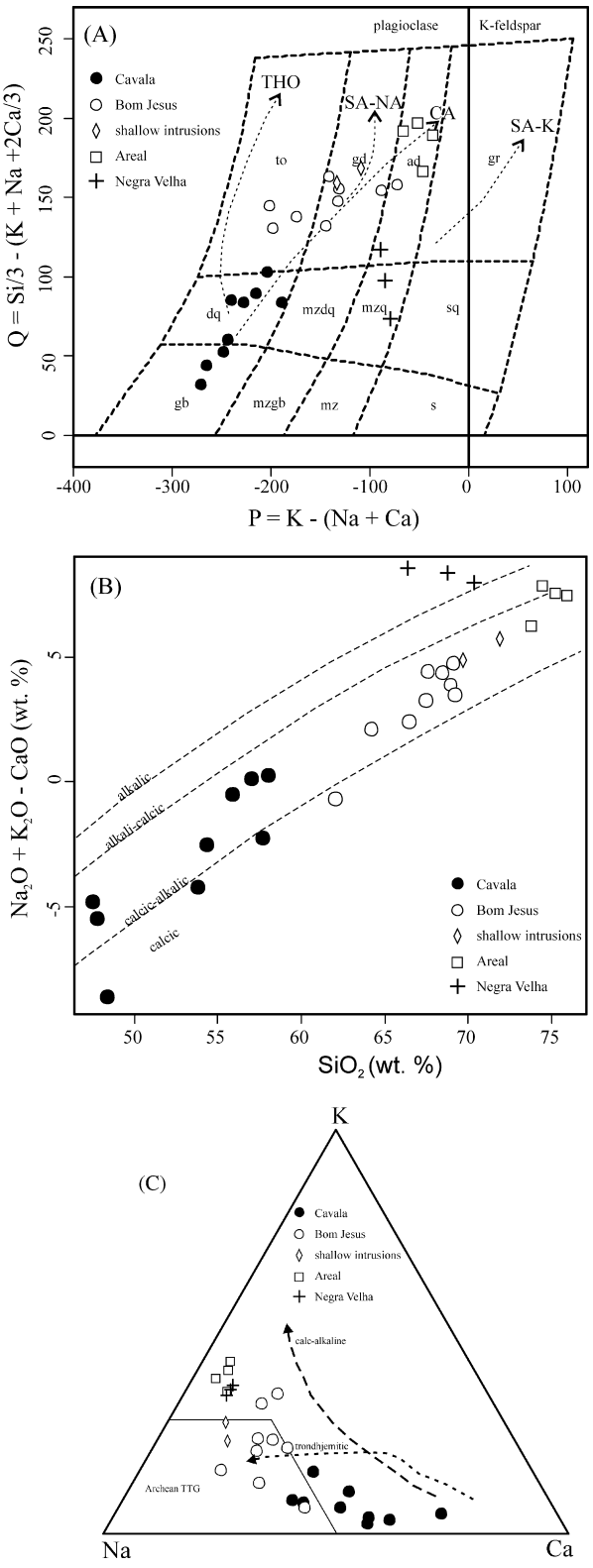


**Fig. 6.** (A) *P*–*Q* cationic diagram of Debon and Le Fort (1988). Labeled arrows (in capitals) indicate the main chemical trends: THO, tholeiitic; CA, calc-alkaline; SA-NA, sodic sub-alkaline; SA-K, potassic sub-alkaline. Rock classification fields (lower case abbreviations) are: to, tonalite; gd, granodiorite; ad, adamellite; gr, granite; dq, quartz diorite; mzdq, quartz monzodiorite; mzq, quartz monzonite; sq, quartz syenite; gb, gabbro; mzgb, monzogabbro; mz, monzonite; s, syenite. (B) $SiO_2$ versus $K_2O + Na_2O$–CaO (Frost et al., 2001), and (C) cationic K–Na–Ca diagram (Nockolds and Allen, 1953; Barker and Arth, 1976). All diagrams plot samples from granitoids of the Tromaí Intrusive Suite and Negra Velha Granite.

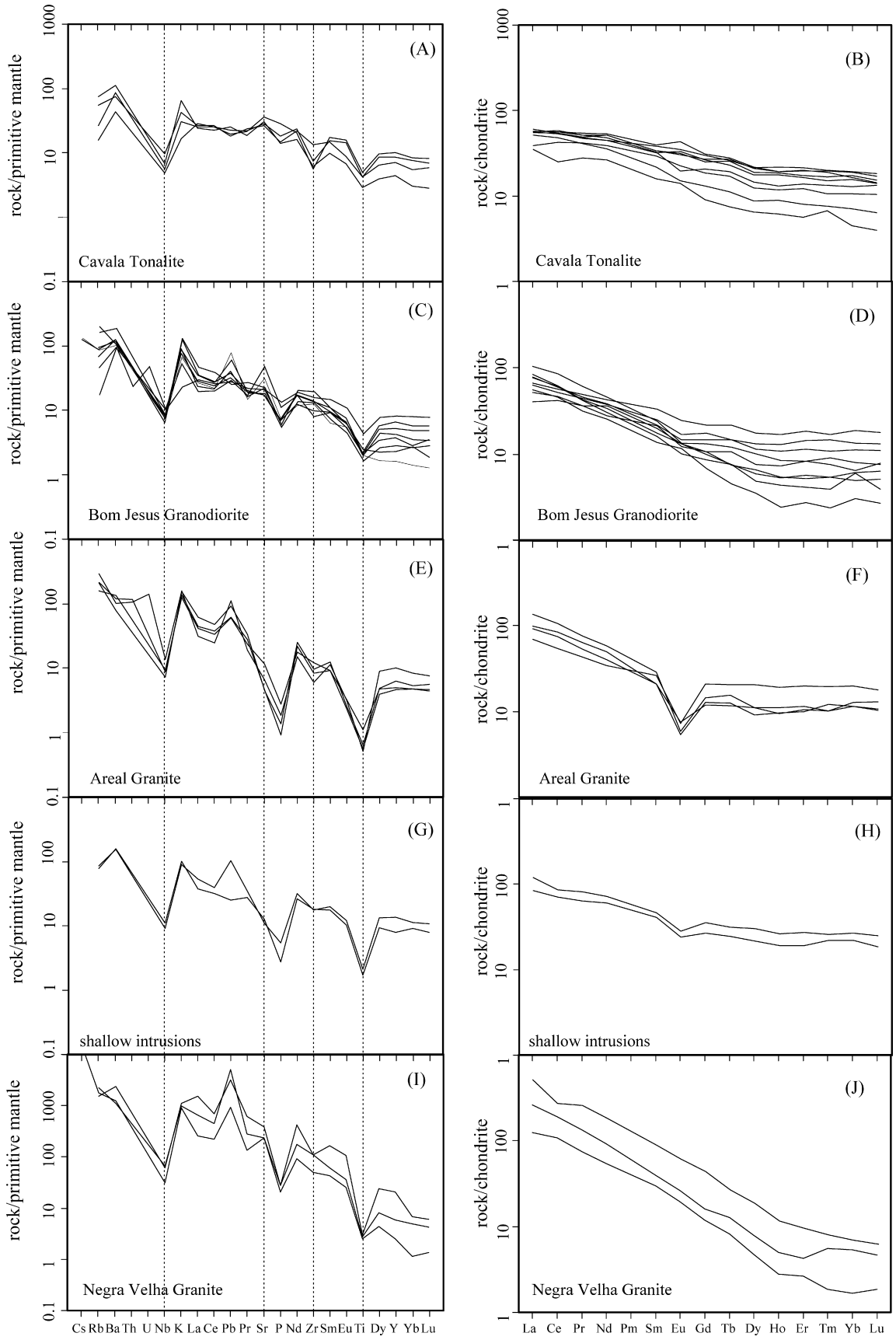


**Fig. 7.** Primitive mantle-normalized (Sun and McDonough, 1989) spidergrams and chondrite-normalized (Boynton, 1984) REE plots for the granitoids of the Tromaí Intrusive Suite and Negra Velha Granite.

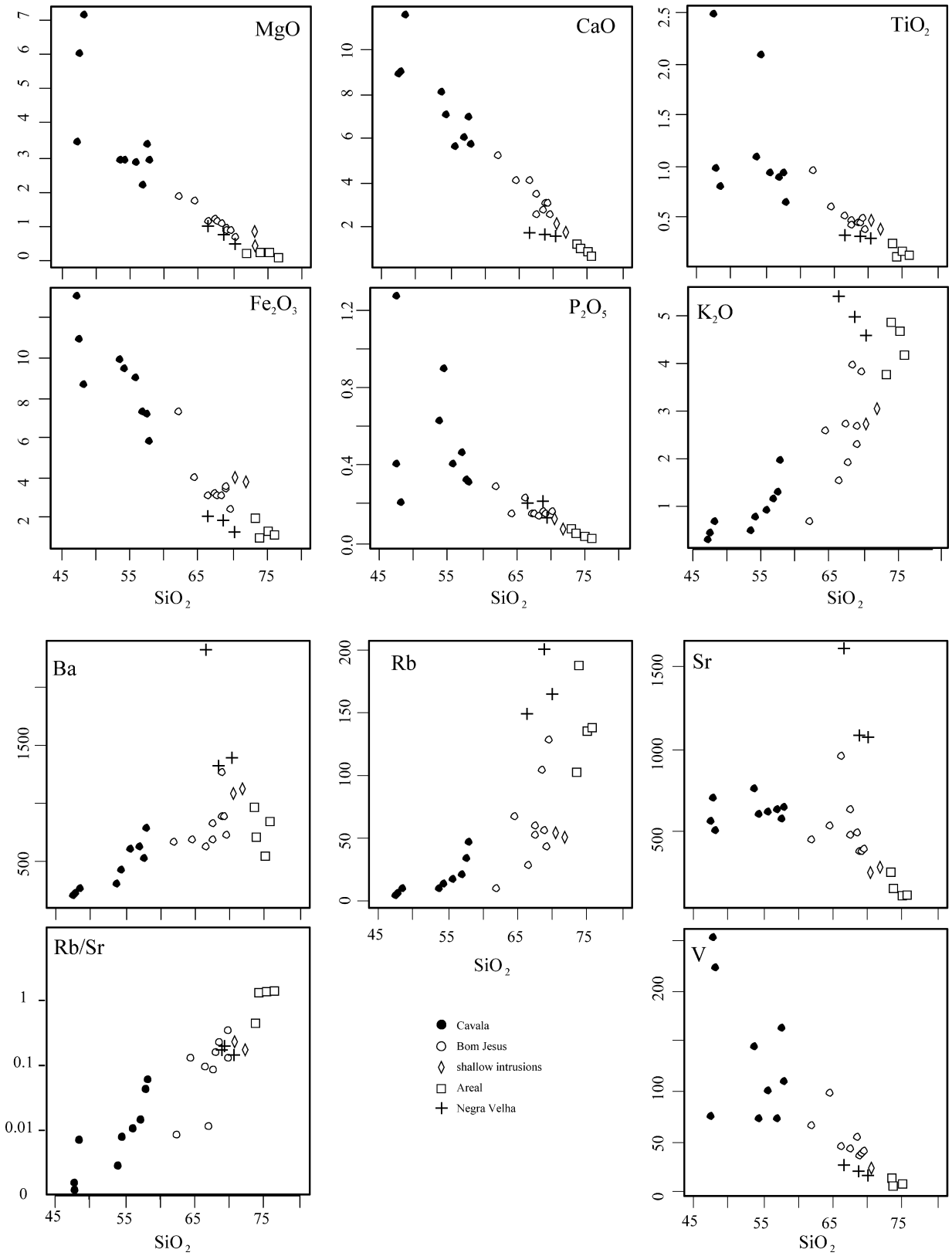


**Fig. 8.** Harker-type diagrams for the granitoids of the Tromaí Intrusive Suite and Negra Velha Granite.

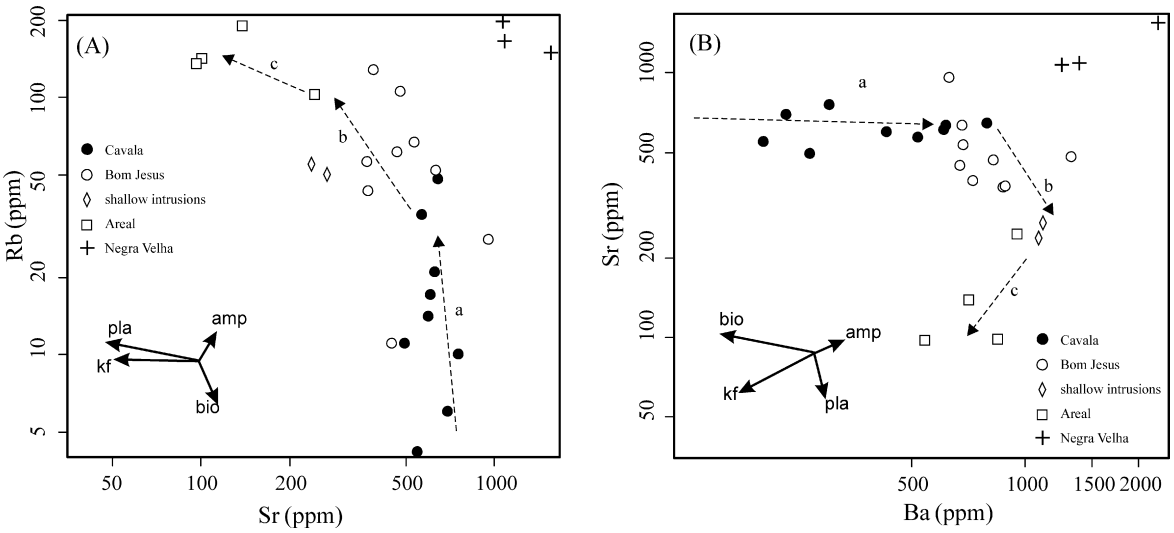


**Fig. 9.** (A) Rb × Sr and (B) Sr × Ba plots for the granitoids of the Tromaí Intrusive Suite and Negra Velha Granite. Dashed arrows labeled "a", "b" and "c" show possible trends that arise from the fractional crystallization controlled by different silicate phases. The solid vectors (according to Dall'Agnol et al., 1999) indicate the main minerals that may control the crystallization. amp, amphibole; bio, biotite; kf, K-feldspar; pla, plagioclase.

observed. Broadly, the REE and multi-element patterns resemble those from the Areal Granite (Fig. 7G and H).

### 5.1.3. Areal Granite

The Areal Granite shows the highest $SiO_2$ concentrations, between 73.4 and 75.9%, and the $K_2O$ contents vary between 3.8 and 4.9%. The $K_2O/Na_2O$ ratios are slightly higher than one, and the sum of $Fe_2O_3 + MgO + TiO_2$ is low, ranging from 1.3 to 1.7% (Table 5c), which is a consequence of the low percentage of mafic minerals. The rocks are also weakly peraluminous, which is compatible with the presence of biotite and the absence of more aluminous minerals.

Among the trace-elements, Ni and V show the lowest values in all studied granitoids, and the Sc concentrations are the lowest within the suite, being similar to those presented by the Negra Velha Granite. The Areal Granite shows a relative depletion in La and Ce in relation to the neighbors K and P, and enrichment in Nd and Sm in relation to Zr (Fig. 7E) when compared to the other types of granitoids. Also, the P and Ti negative anomalies are more pronounced than in other granitoids. The Rb/Sr (>0.4) and Rb/Zr (>0.74) ratios are the highest, whereas the Sr/Y ratios (3–11) are the lowest of all types of granitoids.

The sum of REE concentrations is slightly higher than those of the other granitoids of the same suite and the fractionation between light and heavy REE is moderate (Fig. 7F), with La/Yb(n) ratios of 3.5–10.8, caused by some enrichment in the light REE, since the heavy REE show a flat distribution. A feature that is distinctive of the Areal Granite is the sharp negative Eu anomaly ($Eu/Eu^* = 0.3–0.5$).

## 5.2. Negra Velha Granite

The Negra Velha Granite shows rather restricted chemical composition, with $SiO_2$ ranging from 66.5 to 70.4%, $K_2O$ in the range 4.3–4.5%, $Na_2O$ varying from 4.9 to 5.0%, and CaO contents of 1.5–1.6%. The Negra Velha Granite shows an evolved (Fig. 5B), alkalic (Frost et al., 2001) character (Fig. 6B). The rocks have $Na_2O/K_2O$ ratio of about one, $Fe_2O_3^*/(Fe_2O_3^* + MgO)$ of 0.69–0.75, and are weakly metaluminous. As a rule, the samples of the Negra Velha Granite plot outside the trends formed by the granitoids of the Tromaí Suite in the chemical diagrams (Figs. 5 and 6) and form a distinct association.

The Negra Velha Granite presents the highest Rb, Sr, Ba, and Hf concentrations among all the studied granitoids (Tables 5 and 6), and the Sr and Ba contents are especially high (>1000 ppm). The Zr and Nb contents are also relatively higher than in the Tromaí Suite, whereas the Sc and V concentrations are lower. Furthermore, the Sr/Y and La/Yb(n) ratios are strongly fractionated (Tables 5c and 6).

The trace-elements show enrichment in LIL elements in relation to the HFS elements, which is still higher than what is observed in the Tromaí Suite, with more pronounced positive Nd and Pb anomalies (Fig. 7I). The Negra Velha rocks show moderate REE contents (180–325 ppm), absence of Eu anomaly, and strong fractionation between the light and heavy REE (Fig. 7J), with La/Yb(n) ranging from 49 to 74.

## 6. Petrogenetic aspects of the granitoids

### 6.1. Tromaí Intrusive Suite

In a previous study, Pastana (1995) stated that the Tromaí Suite resembled Archean TTG suites produced by the partial melting of an amphibolitic lower crust. Typically, TTG are low-K, silica-rich (>64%) suites with La/Yb(n) >20 and Yb(n) <8, which show a trondhjemitic magmatic trend and lack mafic end members. These suites are thought to have formed dominantly via low to moderate degree of partial melting (and not fractional crystallization) of hydrated low-K basaltic (subducted) crust at pressures enough to stabilize garnet ± amphibole (see Martin et al., 2005 for review).

In fact, a series of samples of the Tromaí Suite plot on the Archean TTG field in the diagram of Barker and Arth (1976) (Fig. 6C), and samples of the Cavala and Bom Jesus units straddle the fields of Archean TTG and post-Archean granitoids in the La/Yb(n) versus Yb(n) diagram of Martin (1994) (not shown). However, the behavior observed in Fig. 6C may be interpreted as Na-enrichment of a calc-alkaline suite, since the whole set of analyzed samples of the Tromaí Suite display a continuous trend towards the K apex. In addition, the Tromaí Suite shows a wider range of $SiO_2$ content, La/Yb(n) 3–18, Yb(n) <10, and is dominantly medium-K, which are aspects that differ from those of Archean TTG granitoids. Furthermore, the granitoids lack xenoliths of mafic-ultramafic rocks and show basic end-members. Moreover, the compositional variation of the granitoids observed on silica variation diagrams show lin-

ear trends (Fig. 8), which are typical of calc-alkaline suites. These trends are generally characterized by negative correlation between the $SiO_2$ contents and those of MgO, CaO, $TiO_2$, $Fe_2O_3$, and $P_2O_5$, and positive correlation between $SiO_2$ and $K_2O$ and between $SiO_2$ and the Rb/Sr ratio. There is also a general, not necessarily linear, increase in the Ba and Rb, and decrease in the Sr and V concentrations with increasing $SiO_2$ contents.

Although clots of mafic minerals and microgranular enclaves of mineralogical composition similar to that of the Cavala unit are frequent, the granitoids of the Tromaí Intrusive Suite do not show xenoliths of the country rocks. This observation, in addition to the Nd isotope evidence, and to the gradual transition between the different units of the suite suggest that wall-rock assimilation and magma mixing-mingling were not important processes (e.g., Dall'Agnol et al., 1999) in the magmatic evolution of the suite. Instead, magmatic differentiation appears to explain better the characteristics of the Tromaí granitoids, which may occur through fractional crystallization and/or variable degrees of partial melting.

As regards the two mechanisms of differentiation, the Tromaí Suite shows a rather complex behavior. The trends observed in the Harker diagrams (Fig. 8) are compatible with fractional crystallization controlled by different mafic and felsic mineral phases that accompanies the increase in the $SiO_2$ concentration. Fractional crystallization is also evident in the Rb versus Sr and Sr versus Ba diagrams (Fig. 9A and B) that show vectors indicating the changes in the residual liquid composition in response to the fractionation of mineral phases such as plagioclase, K-feldspar, amphibole, and biotite (e.g., Hanson, 1978; Dall'Agnol et al., 1999; Barr et al., 2001). These two diagrams suggest three evolutionary trends for the Tromaí Suite granitoids: (a) simultaneous fractionation of plagioclase and amphibole; (b) plagioclase-dominated fractionation with subordinate influence of amphibole and K-feldspar; (c) plagioclase fractionation with higher influence of K-feldspar, which is more evident in Fig. 9B. Also, Ni decreases from 17 ppm at mg# 51 to 1–3 ppm at mg# 10–20 (figure not shown), which might indicate separation of olivine during the evolution of the suite. Furthermore, fractionation controlled by silicate minerals is also indicated by global increase in the REE abundance with increasing $SiO_2$ concentration, although the REE patterns are not necessarily parallel.

However, the distribution of, and relationships between, some trace-elements of the Tromaí Intrusive Suite are not always equivocal. As a rule, the residual liquid produced by fractional crystallization is depleted in compatible elements whereas it is enriched in these elements when partial melting is the differentiation process. As a consequence, liquids produced by fractional crystallization yield vertical trends in logarithmic plots whereas those produced by partial melting will show a flat distribution (e.g., Cocherie, 1986; Martin, 1994; Souza et al., 2007). In this aspect, the Rb versus V, and Rb versus Ni diagrams (Fig. 10) are not clear with respect to the two mechanisms.

Considering that the Tromaí granitoids do not show systematic younging from Na-rich to K-rich granitoids, although the more primitive Cavala granitoids yielded ages older than 2160 Ma (Table 2), it is possible that simple fractionation has not occurred. An alternative explanation for the geochemical data of the Tromaí Suite (see also Barr et al., 2001) is that separate magma batches were produced by different degrees of partial melting of a single, or similar, sources (which is favored by the small variation in the Nd isotope data) and then underwent internal fractional crystallization yielding the different granitoid types within the suite.

Another issue that must be addressed is the source (or sources) of magma that produced the Tromaí granitoids. The presence of igneous microgranular enclaves, the metaluminous character, and

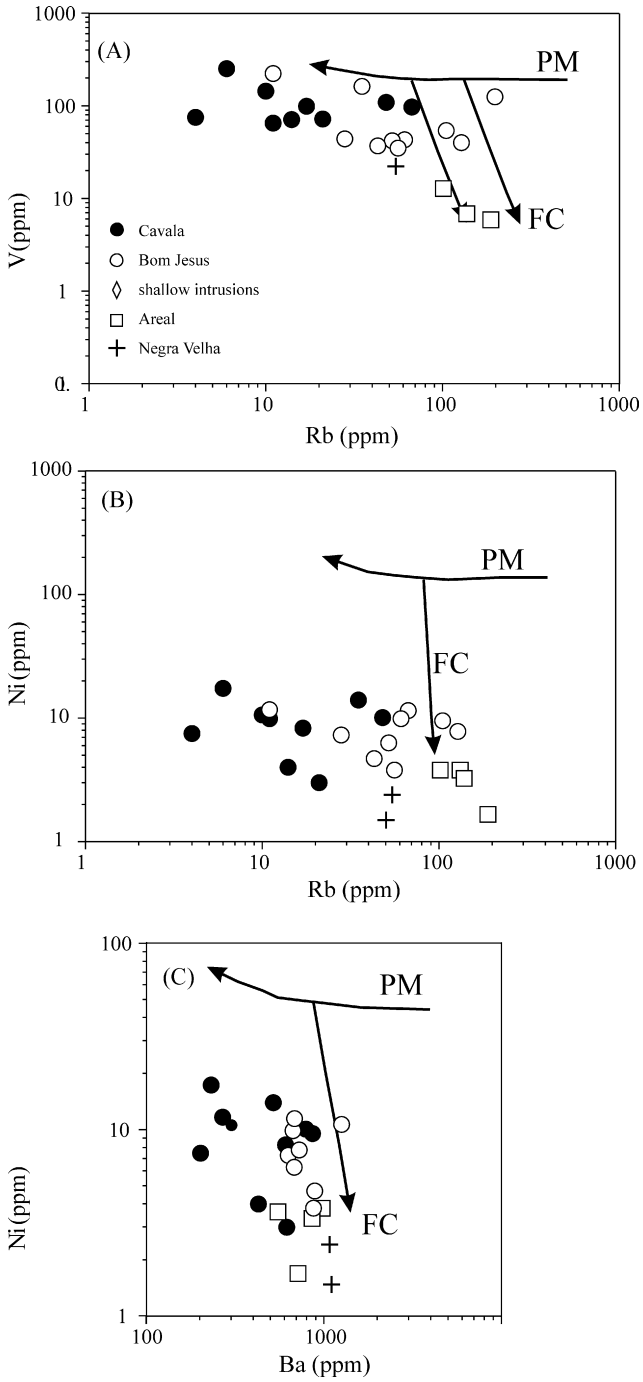


**Fig. 10.** Log–Log plots showing the distribution of compatible versus incompatible trace-elements of granitoids of the Tromaí Intrusive Suite. The PM and FC labels indicate evolution via partial melting and fractional crystallization trends, respectively.

the presence of amphibole indicate deep seated sources, at least for the Cavala type. The geochronological and Nd isotope data clearly indicate juvenile protoliths for the whole suite. Juvenile sources for granitoids might be: (1) subducted materials, including the MORB and/or the young and hot portion of the oceanic crust (Drummond and Defant, 1990; Tarney and Jones, 1994; Whalen et al., 1999) and sediments; (2) mantle-derived materials that could be a MORB-like depleted mantle or LILE-enriched mantle wedge (Martin, 1994); (3) reworked newly formed juvenile continental crust in island arc settings (Barbarin, 1999; Whalen et al., 1999).

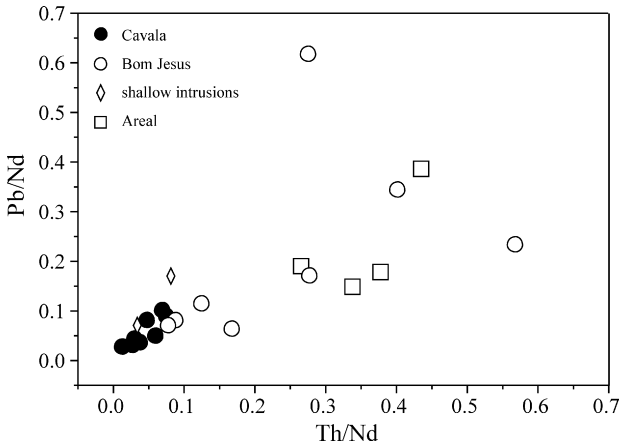


**Fig. 11.** Pb/Nd versus Th/Nd plot for the granitoids of the Tromaí Intrusive Suite. The positive correlation suggests addition of sedimentary-derived silicate melt to an enriched mantle wedge during subduction (Gomez-Tuena et al., 2007).

Melts derived from subduction of the oceanic plate produce granitoids characterized by high Ba/La, Sr/Y (>40), and La/Yb(n) (>12) ratios, and high concentrations of K, Rb, Ba, and Cs. In addition, the Sr/Y would show enrichment trends in relation to Rb and Ba (Drummond and Defant, 1990; Stern and Killian, 1996; Whalen et al., 1999). Granitoids derived from mantle materials show lower Sr/Y (<40) and La/Yb(n) (<12), low Sr (<300 ppm) and high LILE contents, in addition to very low Rb/Sr and Rb/Zr ratios. Furthermore, the presence of basic variants ($SiO_2$ <50 wt.%) indicates direct contribution from the mantle. Crustal materials are enriched in K and Rb, in addition to U and Th. Therefore, the granitoids of the Tromaí Suite, especially the Cavala and Bom Jesus units, display characteristics that are consistent with both oceanic plate- and mantle-derived melts and none of these sources explain alone the geochemical characteristics found in the suite. Furthermore, the positive correlation observed in the Pb/Nd versus Th/Nd plot (Fig. 11) suggests addition of sedimentary-derived silicate melt to an enriched mantle wedge during subduction (e.g., Gomez-Tuena et al., 2007). If the LILE-enriched geochemistry of the Areal Granite is reflecting the participation of some crustal materials in its formation, on the other hand the positive $\varepsilon$Nd values and the absence of significant age difference between the evolved Areal and the more primitive Cavala type indicate that juvenile mantle/ocean plate are still the main source(s) of the Areal Granite magma, in addition to detritus originated from the reworking of early phases of the arc development.

### 6.2. Negra Velha Granite

The analyses of the Negra Velha Granite samples have been plot in the same diagrams of the Tromaí Suite samples (Figs. 5, 6 and 9), and they plot clearly outside the evolutionary trends of this suite, indicating that the two granitoid associations are not co-magmatic, which is confirmed by the age difference between the two units. In addition, the Negra Velha Granite shows an alkalic and not calc-alkaline affinity. However, despite this alkalic affinity and despite the fact that the samples of the Negra Velha Granite plot in the field of the A2-type of Eby (1992) and straddle the limit of the fields of A-type and other granitoid types in the diagram of Whalen et al. (1987) (figures not included), they plot clearly outside the field of A-type granites according to criteria of Dall'Agnol and Oliveira (2007) (Fig. 12), because of the low $Fe_2O_3^*/(Fe_2O_3^* + MgO)$ ratios and high alumina contents. Furthermore, the Negra Velha Granite also differs from A-type granites in other aspects, which include: (1) the strong fractionation between light and heavy rare earth elements, (2) absence of pronounced Eu anomaly, and (3) very high Sr and Ba contents.

Geochemical evidence, such as the high alkali contents ($K_2O + Na_2O$ >5%), low $TiO_2$ content, high Th/Yb ratios, very high concentrations of Rb–Sr–Ba, and the strong fractionation between light and heavy rare earth elements, are compatible with characteristics shown by shoshonitic rocks (Nardi, 1986). However, shoshonites are usually richer in $K_2O$, and have higher $K_2O/Na_2O$ ratio than the Negra Velha samples. Also, the chemical and age differences between the Negra Velha and Tromaí units likely rule out a shoshonitic affinity. The high Ba, Sr and $K_2O$ concentrations, the strong LREE enrichment and the absence of Eu anomalies are consistent with characteristics observed in Archean sanukitoids. However, the relatively high Rb/Sr ratios (>0.1), the low concentrations of Ni and Cr, and, especially, the low mg# (~0.4) rule out a classification of the Negra Velha Granite as a sanukitoid suite as defined by Stern et al. (1989).

As a preliminary assessment, we interpret the Negra Velha Granite to be relatively potassic and alkalic intrusions that occurred late in the magmatic evolution of the São Luís cratonic fragment (see below). The highly evolved character of the granite and the presence of inherited zircon suggest that the magma formed probably by melting of crustal sources. Alternatively, the granite may have formed by partial melting of LILE-enriched mantle-derived materials (e.g., Fig. 13A), with this enrichment occurring in response to previous subduction of oceanic crust or assimilation of crustal rocks. The relatively low $Fe_2O_3^*/(Fe_2O_3^* + MgO)$ ratios and the pres-

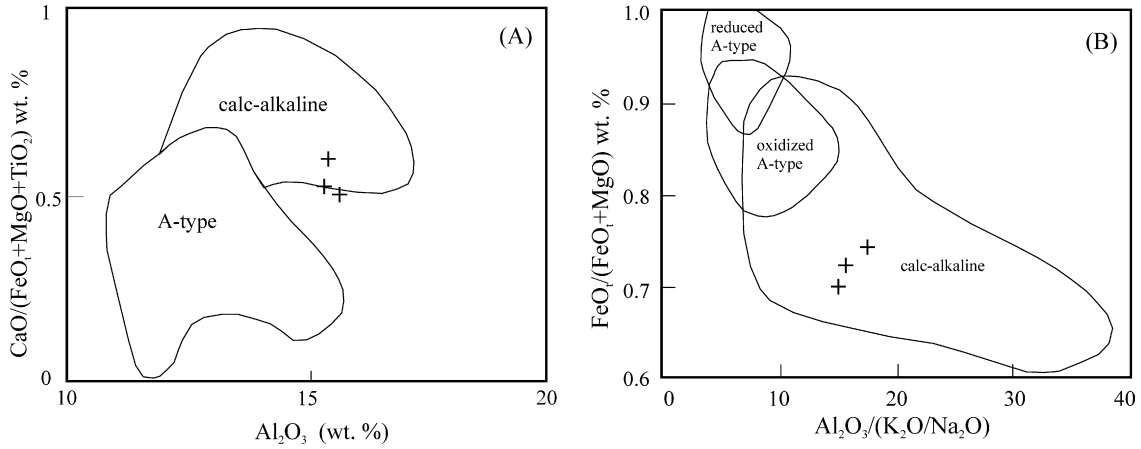


**Fig. 12.** Position of the Negra Velha Granite samples in relation to the fields of A-type and calc-alkaline granitoids in the major-element diagrams of Dall'Agnol and Oliveira (2007).

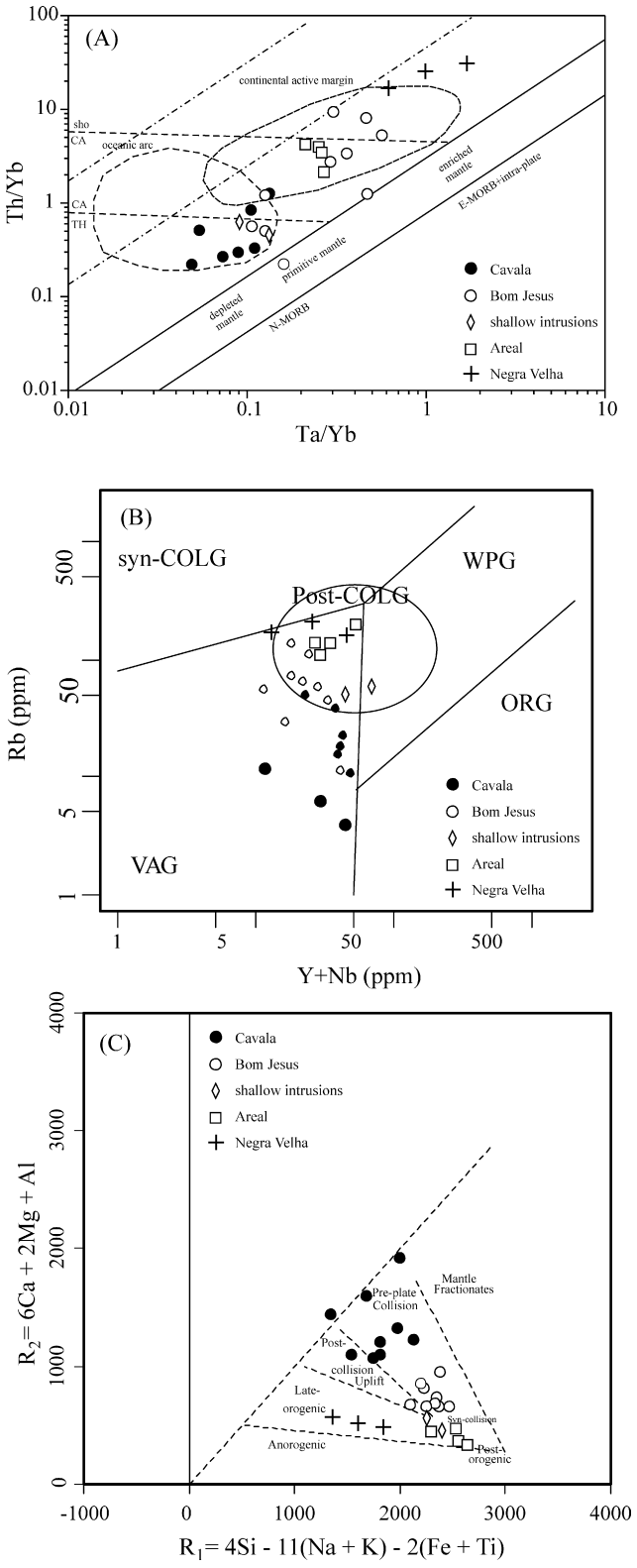


**Fig. 13.** Tectonic discriminant diagrams for the granitoids of the Tromaí Intrusive Suite and Negra Velha Granite. (A) Ta/Yb × Th/Yb plot combining the fields proposed by Pearce (1982) (heavy and dashed lines) and those from Gorton and Schandl (2000) (dotted lines); (B) Rb × Y + Nb plot of Pearce et al. (1984); (C) R1–R2 cationic plot of Batchelor and Bowden (1985).

ence of titanite and opaque minerals indicate that the magma evolved in oxidized conditions.

## 7. Tectonic setting and crustal evolution

Klein et al. (2005a) stated that the present-day configuration of the São Luís cratonic fragment resulted from at least three periods of rock formation, occurring at ~2240 Ma, 2168–2147 Ma, and 2090 Ma, and that more than 90% of the exposed cratonic rocks were derived from juvenile protoliths. More recently, Klein et al. (2008b) refined the timing and tectonic setting of the volcanic events that took place in the cratonic area and described orogenic volcanism occurring 2240 Ma and 2164–2160 Ma ago in addition to a poorly constrained pulse occurred at about 2068 Ma. Adding the results presented in this paper, the previous interpretations are broadly valid, but our findings bring new insights into the understanding of the crustal evolution of the cratonic area.

The timing of magmatic activity recognized so far in the São Luís cratonic fragment is summarized in Fig. 14, along with the range of crustal residence ages ($T_{DM}$) for the majority of this magmatism. An early phase of ocean basin (or continental margin?) and arc development commenced prior to 2260 Ma, and is represented by the metavolcano-sedimentary Aurizona Group of 2240 Ma. This is indicated by the age of the oldest zircon found in the metavolcano-sedimentary association. The Aurizona Group contains arc-related calc-alkaline metapyroclastic rocks formed from juvenile protoliths in addition to minor older crustal components (Fig. 14) and mafic tholeiitic and ultramafic metavolcanic rocks with chemical signature of back arc and/or island arc setting (Klein et al., 2008a). The sedimentary portion of this group is dominated by quartzites and pellites, and carbonate rocks are not observed. This supracrustal sequence was intruded by a small pluton of granophyric rocks at 2114 ± 3 Ma (Klein et al., 2008b).

The calc-alkaline granitoids of the Tromaí Suite occupy the majority of the exposed Pre-Cambrian terrane (Figs. 1 and 2), indicating that most of the São Luís crust is juvenile and formed mainly in the Rhyacian period between ~2170 Ma and 2150 Ma (Fig. 14). The concentration, distribution and some elemental ratios presented by the trace-elements of the analyzed samples of the Tromaí Suite display orogenic signatures compatible with subduction (volcanic-arc/island arc rocks; Fig. 13), notably the Cavala and Bom Jesus types. Especially, the calc-alkaline character and the negative Nb anomaly along a wide range of $SiO_2$ contents (47–72 wt%), the relatively narrow time interval of felsic magmatism, and the Nd isotope evidence pointing to juvenile protoliths are also in keeping with a subduction-related setting. Furthermore, the observed contributions from slab melt components to the granitoids would indicate the subduction of hot, young oceanic crust usually found in back-arc basins rather than in the margins of major ocean basins (Whalen et al., 1999). Therefore, most of the Tromaí Suite records intra-oceanic setting.

The more evolved character of the Areal Granite may be ascribed to a larger participation of crustal materials in the genesis of this granite type. These crustal materials, however, are not much older than the Areal Granite itself, and may be represented by earlier phases of the Tromaí Suite and by erosive products of the volcano-sedimentary sequence, i.e., they might come from the reworking of the island arc, representing the changing of the magma source from the subduction zone (ocean plate and/or mantle wedge) to the island arc. Alternatively, it could represent continental active margin magmatism (Fig. 13).

Tholeiitic basalts and normal- to high-K calc-alkaline andesites of 2164 ± 3 Ma formed in mature arc or active continental margin from juvenile protoliths along with subordinate older (Paleo-

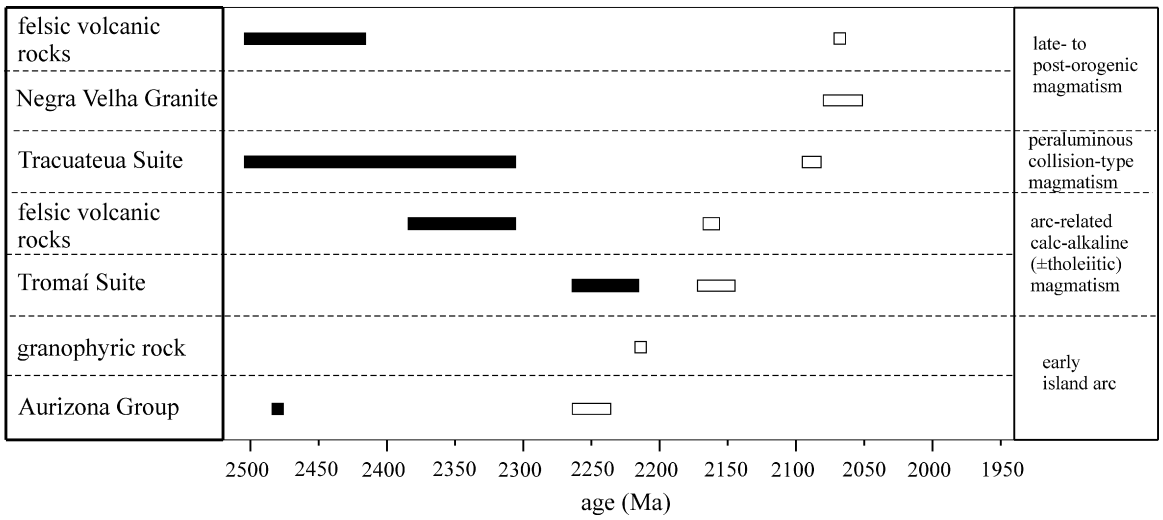


**Fig. 14.** Summary of available crystallization (white bars) and crustal residence (black bars: Nd $T_{DM}$) ages for the magmatic events recognized in the São Luís cratonic fragment (references in the text).

proterozoic) crust. This volcanism is coeval within error with medium-K, calc-alkaline rhyolite, dacite and tuffs of 2160 ± 8 Ma formed in continental margin setting (Fig. 14) from reworked Paleoproterozoic crust (island arc) with incipient Archean contribution (Klein et al., 2008a).

The next event recognized in the São Luís cratonic fragment is the formation of the Tracuateua Suite at 2086–2091 Ma (Palheta, 2001), which has been described by Lowell (1985) as composed of peraluminous S-type granitoids. Although lacking geochemical data, similar and coeval (2100–2080 Ma) magmatism, i.e., muscovite-bearing leucogranites have been described in the basement of the Gurupi Belt (Palheta, 2001; Klein et al., 2005b). These granitoids record some involvement of older crustal components in their genesis and are interpreted to be collision-type rocks. As such, a continent or continental block, probably having remnants of Archean crust of still unknown origin might have existed to the south-southwestern (to date, the only recognized Archean unit in this region is the Igarapé Grande Metatonalite of 2594 ± 3 Ma that occurs as small lenses in the basement of the Gurupi Belt: Klein et al., 2005b). This inferred continent has rifted to form the ocean basin/continental margin in which formed the island arc described above. This island arc amalgamated to this continental block by ~2100–2080 Ma.

The granitoids of the Negra Velha unit occupy the field of post-collisional + volcanic-arc granites of Pearce (1996), close to the limit with the field of syn-collisional granites (Fig. 13B). They also plot in the field of late-orogenic granitoids in the diagram of Batchelor and Bowden (1985) (Fig. 13C). These geochemical characteristics are in keeping with field and geochronological information that suggest a late- to post-orogenic timing for the Negra Velha Granite (2056–2076) (Fig. 14), associated with an extensional event. Weakly peraluminous, medium-K, calc-alkaline dacite and tuff of 2068 Ma (Klein et al., 2008a) and formed from reworked crustal protoliths (Fig. 14) are also related to this phase.

## 8. Global implications

Our results and understanding about the crustal evolution of the São Luís cratonic fragment have also continental- and worldwide significance. The time interval in which formed most of the rock associations of the São Luís cratonic fragment falls within the early stage (2.2–2.15 Ga) of the main period of juvenile crustal growth in the South American Platform (ca. 2.2–2.0 Ga, Cordani and Sato, 1999), which is coincident with the period of the Trans-Amazonian cycle of orogenies of the Amazonian Craton (e.g., Hurley et al., 1968).

Santos et al. (2003), based on data published in Klein and Moura (2001), considered the São Luís Craton as the type-area of the Trans-Amazon orogen. We cannot discard this working hypothesis, however, as discussed by Klein and Moura (2008 and many references therein), the São Luís "Craton" bears abundant resemblances to the juvenile Eburnean-Birimian terranes of the West-African Craton, including the rock types and associations, tectonic settings, and the age of tectonic and magmatic events. Therefore, São Luís is most likely a fragment of the West-African Craton that was left behind in the South American Platform after the break-up of the Pangea supercontinent in Mesozoic times. Parts of this cratonic fragment are concealed under the Phanerozoic sedimentary cover and parts have been reworked during the Neoproterozoic Era and are now included in the basement of orogenic belts related to the Brasiliano/Pan-African cycle of orogenies, such as the Gurupi (Fig. 1) and Borborema belts (Klein et al., 2005b; Klein and Moura, 2008; Santos et al., 2008).

The age and Nd isotope patterns showed by the Tromaí Intrusive Suite (and by the volcanic and metavolcanic rocks addressed by Klein et al., 2008a, Fig. 14) overlap the end of the 2.4–2.2 Ga period in which the production rate of juvenile continental crust is considered to be less than the background rate, contrasting with periods of worldwide peaks of crustal growth that occurred at 2.5 Ga and 1.9 Ga (Condie, 2000). However, combining U–Pb and Lu–Hf systematics on detrital zircon crystals from different continents, Condie et al. (2005) argued that this low rate might reflect inadequate sampling of detrital zircon populations and/or extensive reworking of 2.4–2.2 Ga crust, or that this crust could be hidden under sedimentary covers, ice camps and jungle. This interpretation is corroborated by our data and, although subordinate, by rock units from the Bacajá (Vasquez, 2006) and Carecuru (Rosa-Costa et al., 2006) domains of the Amazonian Craton, and granitoids of the Dabakala region of the West-African Craton (Gasquet et al., 2003).

Finally, the juvenile granitoid magmatism documented in this study bears also many similarities with the characteristics presented by granitoid rocks of the younger (1.92–1.83 Ga) Flin Flon-Snow Lake Belt of the Trans-Hudson Orogen in Canada, which is taken as the type example of Paleoproterozoic juvenile arc

produced by modern-style plate tectonics (e.g., Whalen et al., 1999).

## 9. Conclusions

As a concluding summary of our observations and interpretations on two distinct granitoid associations of the São Luís cratonic fragment, we can list the following:

(1) The Tromaí Intrusive Suite is an expanded suite of subordinate basic to predominantly acid, low- to high-K, and metaluminous to weakly peraluminous calc-alkaline granitoids, which is subdivided into three types, named Cavala Tonalite, Bom Jesus Granodiorite, and Areal Granite (from the more primitive to the more evolved phases).
(2) The Tromaí Suite formed between 2168 Ma and 2147 Ma ago from magmas derived from juvenile sources that include oceanic plate, mantle wedge, in addition to minor recycled early-Paleoproterozoic materials (arc sediments).
(3) The magmatic differentiation process that gave rise to the Tromaí Suite was fractional crystallization, possibly combined with small degrees of partial melting.
(4) The juvenile character and the geochemical signature of the Tromaí Suite reflect an intra-oceanic setting that transitioned to continental margin. This transition is better represented by coeval felsic to intermediate volcanism (2164–2160 Ma) described in Klein et al. (2008a).
(5) The tectonic setting and magmatic processes are similar to those operating in modern-style plate tectonics.
(6) The Negra Velha Granite forms a distinct association of alkali- and Rb-Sr-Ba-rich granitoids that intruded 2056–2076 Ma ago and records the post-tectonic phase of the orogenesis (2240–2080 Ma) that built up the São Luís cratonic fragment.

## Acknowledgements

This paper is an outcome of the Carutapera project that was conducted by CPRM/Geological Survey of Brazil from 2004 to 2006, and the authors acknowledge the contributions of P.A.C. Marinho (*in memoriam*), J.H. Larizzatti, L.T. Rosa-Costa, D.C. Lobato, and M.T.L. Faraco (CPRM) during the execution of the project. Discussions with Marcelo Vasquez (CPRM) and Roberto Dall'Agnol (UFPA) are also appreciated. E.L.K. acknowledges the Brazilian agency "Conselho Brasileiro de Desenvolvimento Científico e Tecnológico" (CNPq) for a research grant (process 308994/2006-0). The authors are grateful to two anonymous reviewers, whose suggestions greatly improved the original manuscript.

## Appendix A. Summary of analytical procedures

U–Pb SHRIMP analyses were undertaken on SHRIMP II and RG of the Research School of Earth Sciences of the Australian National University, Canberra, Australia. Zircon crystals were hand-picked, mounted in epoxy resin, ground to half-thickness, and polished with diamond paste; a conductive gold-coating was applied just prior to analysis. SHRIMP analytical procedures followed the methods described in Compston et al. (1984) and Williams (1998). Raw data were reduced using the Squid program (Ludwig, 2001), and age calculations and concordia plots were done using both Squid (Ludwig, 2001) and Isoplot/Ex software (Ludwig, 2003). Analyses for individual SHRIMP spots are plotted on concordia diagrams with 1s uncertainties. Where data are combined to calculate an age, the quoted uncertainties are at 95% confidence level, with uncertainties in the U–Pb standard calibration included in any relevant U–Pb intercept and concordia age calculations.

Zircon dating by the Pb evaporation method (Kober, 1986) was conduced at the Laboratório de Geologia Isotópica (Pará-Iso) of the Universidade Federal do Pará, Belém, using the double filament array. Isotopic ratios were measured in a FINNIGAN MAT 262 mass spectrometer and data were acquired in the dynamic mode using the ion-counting system of the instrument. For each step of evaporation, a step age is calculated from the average of the $^{207}Pb/^{206}Pb$ ratios. When different steps yield similar ages, all are included in the calculation of the crystal age. If distinct crystals furnish similar mean ages, then a mean age is calculated for the sample. Crystals or steps showing lower ages probably reflect Pb loss after crystallization and are not included in sample age calculation. Common Pb corrections were made according to Stacey and Kramers (1975) and only blocks with $^{206}Pb/^{204}Pb$ ratios higher than 2500 were used for age calculations. $^{207}Pb/^{206}Pb$ ratios were corrected for mass fractionation by a factor of 0.12% per a.m.u, given by repeated analysis of the NBS-982 standard, and analytical uncertainties are given at the $2\sigma$ level.

Whole rock powders were analyzed by ICP-ES for major elements and ICP-MS for trace-elements, including the rare-earth elements, at the Acme Analytical Laboratories Ltd. in Canada. Chemical diagrams were mostly generated using the GCDkit software (Janousek et al., 2003).

## References

Barbarin, B., 1999. A review of the relationships between granitoid types, their origins and their geodynamic environments. Lithos 46, 605–626.
Barker, F., Arth, J.G., 1976. Generation of trondhjemitic-tonalitic liquids and Archaean bimodal trondhjemite-basalt suites. Geology 4, 596–600.
Barr, S.M., White, C.E., Culshaw, N.G., Ketchum, J.W.F., 2001. Geology and tectonic setting of Paleoproterozoic granitoid suites in the Island Harbour Bay area, Makkovik Province, Labrador. Can. J. Earth Sci. 38, 441–463.
Batchelor, R.A., Bowden, P., 1985. Petrogenetic interpretation of granitic rock series using multicationic parameters. Chem. Geol. 48, 43–55.
Boynton, W.V., 1984. Cosmochemistry of the rare-earth elements: meteorite studies. In: Henderson, P. (Ed.), Rare-Earth Elements Geochemistry. Elsevier, Amsterdam, pp. 63–114.
Cocherie, A., 1986. Systematic use of trace element distribution patterns in log-log diagrams for plutonic suites. Geochim. Cosmochim. Acta 50, 2517–2522.
Compston, W., Williams, I.S., Meyer, C., 1984. U–Pb geochronology of zircons from lunar breccia 73217 using a sensitive high mass-resolution ion-microprobe. J. Geophys. Res. 98B, 525–534.
Condie, K.C., 2000. Episodic continental growth models: afterthoughts and extensions. Tectonophysics 322, 153–162.
Condie, K.C., Beyer, E., Belousova, E., Griffin, W.L., O'Reylly, S.Y., 2005. U–Pb isotopic ages and Hf isotopic composition of single zircons: the search for juvenile Precambrian continental crust. Precamb. Res. 139, 42–100.
Cordani, U.G., Sato, K., 1999. Crustal evolution of the South American Platform, base don Nd isotopic systematics on granitoid rocks. Episodes 22, 167–173.
Costa, J.L., Araujo, A.A.F., Villas Boas, J.M., Faria, C.A.S., Silva Neto, C.S., Wanderley, V.J.R., 1977. Projeto Gurupi. DNPM/CPRM, p. 258.
Dall'Agnol, R., Oliveira, D.C., 2007. Oxidized, magnetite-series, rapakivi-type granites of Carajás, Brazil: implications for classification and petrogenesis of A-type granites. Lithos 93, 215–233.
Dall'Agnol, R., Rämö, O.T., Magalhães, M.S., Macambira, M.J.B., 1999. Petrology of the anorogenic, oxidised Jamon and Musa granites, Amazonian Craton: implications for the genesis of Proterozoic A-type granites. Lithos 46, 431–462.
Debon, F., Le Fort, P., 1988. A cationic classification of common plutonic rocks and their magmatic associations: principles, method, applications. Bull. Miner. 111, 493–510.
Drummond, M.S., Defant, M.J., 1990. A model for trondhjemite-tonalite-dacite genesis and crustal growth via slab melting: Archean to modern comparisons. J. Geophys. Res. 95, 21503–21521.
Eby, N.G., 1992. Chemical subdivision of the A-type granitoids: petrogenetic and tectonic implications. Geology 20, 641–644.
Frost, B.R., Barnes, C.G., Collins, W.J., Arculus, R.J., Ellis, D.J., Frost, C.D., 2001. A geochemical classification for granitic rocks. J. Petrol. 42, 2033–2048.
Gasquet, D., Barbey, P., Adou, M., Paquette, J.L., 2003. Structure, Sr–Nd isotope geochemistry and zircon U–Pb geochronology of the Dabakala area (Côte D'Ivoire): evidence for a 2.3 crustal growth event in the Palaeoproterozoic of West Africa? Precamb. Res. 127, 329–354.

Gomez-Tuena, A., Langmuir, C.H., Goldstein, S.L., Straub, S.M., Ortega-Gutiérrez, F., 2007. Geochemical evidence for slab melting in the Trans-Mexican volcanic belt. J. Petrol. 48, 537–562.
Gorton, M.P., Schandl, E.S., 2000. From continents to island arcs: a geochemical index of tectonic setting for arc-related and within-plate felsic to intermediate volcanic rocks. Can. Miner. 38, 1065–1073.
Hanson, G.N., 1978. The application of trace elements to the petrogenesis of igneous rocks of granitic composition. Earth Planet. Sci. Lett. 38, 26–43.
Hurley, P.M., Melcher, G.C., Pinson, W.H., Fairbairn, H.W., 1968. Some orogenic episodes in South America by K–Ar and whole-rock Rb–Sr dating. Can. J. Earth Sci. 5, 633–638.
Janousek, V., Farrow, C.M., Erban, V., 2003. GCDkit: new PC software for interpretation of whole-rock geochemical data from igneous rocks. Godschmidt Conf. Abstr., A186.
Klein, E.L., Moura, C.A.V., 2001. Age constraints on granitoids and metavolcanic rocks of the São Luís craton and Gurupi belt, northern Brazil: implications for lithostratigraphy and geological evolution. Int. Geol. Rev. 43, 237–253.
Klein, E.L., Moura, C.A.V., 2003. Sintese geológica e geocronológica do Craton São Luís e do Cinturão Gurupi na região do rio Gurupi (NE-Para/NW-Maranhão). Revista Geologia USP, Série Científica, 3, 97–112.
Klein, E.L., Moura, C.A.V., 2008. São Luís craton and Gurupi belt (Brazil): possible links with the West-African craton and surrounding Pan-African belts. In: Pankhurst, R.J., Trouw, R.A.J., Brito Neves, B.B., de Wit, M.J. (Eds.), West Gondwana: Pre-Cenozoic Correlations across the South Atlantic Region, vol. 294. Geological Society, London, pp. 137–151, Special Publications.
Klein, E.L., Moura, C.A.V., Pinheiro, B.L.S., 2005a. Paleoproterozoic crustal evolution of the São Luís Craton, Brazil: evidence from zircon geochronology and Sm–Nd isotopes. Gondwana Res. 8, 177–186.
Klein, E.L., Moura, C.A.V., Krymsky, R., Griffin, W.L., 2005b. The Gurupi belt in northern Brazil: lithostratigraphy, geochronology, and geodynamic evolution. Precamb. Res. 141, 83–105.
Klein, E.L., Larizzatti, J.H., Marinho, P.A.C., Rosa-Costa, L.T., Luzardo, R., Faraco, M.T.L., 2008b. Folha Cândido Mendes – SA.23-V-D-II, Estado do Maranhão, Escala 1:100.000. Geologia e Recursos Minerais, CPRM/Serviço Geológico do Brasil, in press.
Klein, E.L., Luzardo, R., Moura, C.A.V., Lobato, D.C., Brito, R.S.C., Armstrong, R., 2008a. Geochronology, Nd isotopes and reconnaissance geochemistry of volcanic and metavolcanic rocks of the São Luís Craton, northern Brazil: implications for tectonic setting and crustal evolution. J. South Am. Earth Sci, in press.
Kober, B., 1986. Whole-grain evaporation for $^{207}Pb/^{206}Pb$-age-investigations on single zircons using a double-filament thermal ion source. Contrib. Mineral. Petrol. 93, 482–490.
Lameyre, J., Bowden, P., 1982. Plutonic rock type series: discrimination of various granitoid series and related rocks. J. Volcanol. Geothermal Res. 14, 169–186.
Lowell, G.R., 1985. Petrology of the Bragança batholith, São Luís craton, Brazil. In: The crust—the significance of granite-gneisses in the lithosphere. Theophrastus Pub, Athens, pp. 13–34.
Ludwig, K.R., 2001. Squid Version 1.03—A User's Manual. Berkeley Geochronology Center Special Publication, vol. 2, pp. 18.
Ludwig, K.R., 2003. User's manual for Isoplot/Ex version 3.00—A geochronology toolkit for Microsoft Excel. Berkeley Geochronological Center Special Publication, vol. 4, pp. 70.
Martin, H., 1994. The Archean grey gneiss and the genesis of continental crust. In: Condie, K.C. (Ed.), The Archean Crustal Evolution. Elsevier, Amsterdam, pp. 205–259.
Martin, H., Smithies, R.H., Rapp, R., Moyen, J.F., Champion, D., 2005. An overview of adakite, tonalite-trondhjemite-granodiorite (TTG), and sanukitoid: relationships and some implications for crustal evolution. Lithos 79, 1–24.
Nardi, L.V.S., 1986. As rochas granitóides da série shoshonítica. Rev. Bras. Geociências 16, 3–10.
Nardi, L.V.S., Bitencourt, M.F., Plá-Cid, J., 2005. Classificação de granitóides em associações petrogenéticas. In: Congresso Brasileiro de Geoquímica, X. Extended Abstracts (in CD-ROM).
Nockolds, S.R., Allen, R., 1953. The geochemistry of some igneous rocks series. Geochim. Cosmochim. Acta 4, 105–142.
Palheta, E.S.M., 2001. Evolução geológica da região nordeste do Estado do Pará com base em estudos estruturais e isotópicos de granitóides. M.Sc. Thesis. Centro de Geociências, Universidade Federal do Pará, Belém, pp. 143.
Pastana, J.M.N., 1995. Programa Levantamentos Geológicos Básicos do Brasil. Programa Grande Carajás. Turiaçu/Pinheiro, folhas SA.23-V-D/SA.23-Y-B. Estados do Pará e Maranhão. Brasília, CPRM, pp. 205.
Pearce, J.A., 1982. Trace element characteristics of lavas from destructive plate boundaries. In: Thorpe, R.S. (Ed.), Andesites: Orogenic Andesites and Related Rocks. Wiley, Chichester, p. 525.
Pearce, J.A., 1996. Source and settings of granitic rocks. Episodes 19, 120–125.
Pearce, J.A., Harris, N.B.W., Tindle, A.G., 1984. Trace element discrimination diagrams for the tectonic interpretation of granitic rocks. J. Petrol. 25, 956–983.
Peccerillo, A., Taylor, S.R., 1976. Geochemistry of Eocene calc-alkaline volcanic rocks from the Kastamonu area, Northern Turkey. Contrib. Mineral. Petrol. 58, 63–81.
Rosa-Costa, L.T., Lafon, J.M., Delor, C., 2006. Zircon geochronology and Sm-Nd isotopic study: further constraints for the Archean and Paleoproterozoic geodynamical evolution of the southeastern Guiana Shield, north of Amazonian Craton, Brazil. Gondwana Res. 10, 277–300.
Santos, J.O.S., Hartmann, L.A., Bossi, J., Campal, N., Schipilov, A., Piñeyro, D., McNaughton, N.J., 2003. Duration of the Trans-Amazonian cycle and its correlation within South America based on U–Pb SHRIMP geochronology of the La Plata Craton, Uruguay. Int. Geol. Rev. 45, 27–48.
Santos, T.J.S., Fetter, A.H., Neto, J.A.N., 2008. Comparisons between the northwestern Borborema Province, NE Brazil, and the southwestern Pharusian Dahomey Belt, SW Central Africa. In: Pankhurst, R.J., Trouw, R.A.J., Brito Neves, B.B., de Wit, M.J. (Eds.), West Gondwana: Pre-Cenozoic Correlations across the South Atlantic Region, vol. 294. Geological Society, London, pp. 101–120, Special Publications.
Souza, Z.S., Martin, H., Peucat, J.J., Jardim de Sá, E.F., Macedo, M.H.F., 2007. Calc-Alkaline Magmatism at the Archean-Proterozoic Transition: the Caicó Complex Basement (NE Brazil). J. Petrol. 48, 2149–2185.
Stacey, J.S., Kramers, J.D., 1975. Approximation of terrestrial lead isotope evolution by a two-stage model. Earth Planet. Sci. Lett. 26, 207–221.
Stern, A.L., Hanson, G., Shirey, S.B., 1989. Petrogenesis of mantle-derived, LILE-enriched Archean monzodiorites and trachyandesites (sanukitoids) in southwestern Superior Province. Can. J. Earth Sci. 26, 1688–1712.
Stern, C.R., Killian, R., 1996. Role of the subducted slab, mantle wedge and continental crust in the generation of adakites from the Andean Austral Volcanic Zone. Contrib. Mineral. Petrol. 123, 263–281.
Streckeisen, A.L., 1976. To each plutonic rock its proper name. Earth Sci. Rev. 12, 1–33.
Sun, S.S., McDonough, W.F., 1989. Chemical and isotopic systematics of oceanic basalts: implications for mantle compositions and processes. In: Saunders, A.D., Norry, M.J. (Eds.), Magmatism in Ocean Basins, vol. 42. Geological Society of London, pp. 313–345, Special Pub.
Tarney, J., Jones, C.E., 1994. Trace element geochemistry of orogenic igneous rocks and crustal growth models. J. Geol. Soc. Lond. 151, 855–868.
Vasquez, M.L., 2006. Geocronologia em zircão, monazita e granada e isótopos de Nd das associações litológicas da porção oeste do Domínio Bacajá: Evolução crustal da porção meridional da Província Maroni-Itacaiúnas - sudeste do Cráton Amazônico. D.Sc. Thesis. Centro de Geociências, Universidade Federal do Pará, Belém, pp. 212.
Whalen, J.B., Currie, K.L., Chappell, B.W., 1987. A-type granites: geochemical characteristics, discrimination and petrogenesis. Contrib. Mineral. Petrol. 95, 407–419.
Whalen, J.B., Syme, E.C., Stern, R.A., 1999. Geochemical and Nd isotopic evolution of Paleoproterozoic arc-type granitoid magmatism in the Flin Flon Belt, trans-Hudson orogen, Canada. Can. J. Earth Sci. 36, 227–250.
Williams, I.S., 1998. U-Th-Pb geochronology by ion microprobe. In: McKibben, M.A., Shanks III, W.C., Ridley, W.I. (Eds.), Applications of microanalytical techniques to understanding mineralizing processes. Reviews in Economic Geology 7, 1–35.